

This is a repository copy of *A synthesis inversion to constrain global emissions of very short-lived chlorocarbons, dichloromethane and perchloroethylene:dichloromethane, and perchloroethylene*.

White Rose Research Online URL for this paper:

<https://eprints.whiterose.ac.uk/id/eprint/159775/>

Version: Accepted Version

Article:

Claxton, Tom, Hossaini, Ryan, Wilson, Chris et al. (26 more authors) (2020) A synthesis inversion to constrain global emissions of very short-lived chlorocarbons, dichloromethane and perchloroethylene:dichloromethane, and perchloroethylene. *Journal of Geophysical Research: Biogeosciences*. e2019JD031818. ISSN: 2169-8961

<https://doi.org/10.1029/2019JD031818>

Reuse

Items deposited in White Rose Research Online are protected by copyright, with all rights reserved unless indicated otherwise. They may be downloaded and/or printed for private study, or other acts as permitted by national copyright laws. The publisher or other rights holders may allow further reproduction and re-use of the full text version. This is indicated by the licence information on the White Rose Research Online record for the item.

Takedown

If you consider content in White Rose Research Online to be in breach of UK law, please notify us by emailing eprints@whiterose.ac.uk including the URL of the record and the reason for the withdrawal request.

Claxton Tom (Orcid ID: 0000-0002-8766-3370)
Hossaini Ryan (Orcid ID: 0000-0003-2395-6657)
Wilson Chris (Orcid ID: 0000-0001-8494-0697)
Montzka Stephen, A. (Orcid ID: 0000-0002-9396-0400)
Chipperfield Martyn, P. (Orcid ID: 0000-0002-6803-4149)
Wild Oliver (Orcid ID: 0000-0002-6227-7035)
Carpenter Lucy, J. (Orcid ID: 0000-0002-6257-3950)
Andrews Stephen, Joseph (Orcid ID: 0000-0002-1918-9419)
Hackenberg Sina, Corinna (Orcid ID: 0000-0002-2165-8827)
Muhle Jens (Orcid ID: 0000-0001-9776-3642)
Park Sunyoung (Orcid ID: 0000-0002-7506-5752)
Atlas Elliot, L. (Orcid ID: 0000-0003-3847-5346)
Schauffler Sue, M. (Orcid ID: 0000-0002-4516-3378)
Vollmer Martin, K. (Orcid ID: 0000-0001-5569-9718)
Schuck Tanja, J. (Orcid ID: 0000-0002-1380-3684)
Engel Andreas (Orcid ID: 0000-0003-0557-3935)
Krummel Paul, B (Orcid ID: 0000-0002-4884-3678)
Yokouchi Yoko (Orcid ID: 0000-0001-6376-8146)
O'Doherty Simon (Orcid ID: 0000-0002-4051-6760)
Young Dickon (Orcid ID: 0000-0002-6723-3138)

This article has been accepted for publication and undergone full peer review but has not been through the copyediting, typesetting, pagination and proofreading process which may lead to differences between this version and the Version of Record. Please cite this article as doi: 10.1029/2019JD031818

A synthesis inversion to constrain global emissions of very short-lived chlorocarbons, dichloromethane and perchloroethylene

Tom Claxton¹, Ryan Hossaini¹, Chris Wilson^{2,3}, Stephen A. Montzka⁴, Martyn P. Chipperfield^{2,3}, Oliver Wild¹, Ewa Bednarz¹, Lucy Carpenter⁵, Stephen Andrews⁵, Sina Hackenberg⁵, Jens Mühle⁶, David Oram⁷, Sunyoung Park⁸, Mi-Kyung Park⁸, Elliot Atlas⁹, Maria Navarro^{9†}, Sue Schauffler¹⁰, David Sherry¹¹, Martin Vollmer¹², Tanja Schuck¹³, Andreas Engel¹³, Paul B. Krummel¹⁴, Michela Maione¹⁵, Jgor Arduini¹⁵, Takuya Saito¹⁶, Yoko Yokouchi¹⁶, Simon O'Doherty¹⁷, Dickon Young¹⁷ and Chris Lunder¹⁸

¹Lancaster Environment Centre, Lancaster University, Lancaster, UK.

²School of Earth and Environment, University of Leeds, Leeds, UK.

³National Centre for Earth Observation, University of Leeds, Leeds, UK.

⁴National Oceanic and Atmospheric Administration, Boulder, Colorado, USA.

⁵Wolfson Atmospheric Chemistry Laboratories, School of Chemistry, University of York, York, UK.

⁶Scripps Institution of Oceanography, University of California, San Diego, California, USA

⁷School of Environmental Sciences, University of East Anglia, Norwich, UK.

⁸Kyungpook Institute of Oceanography, Kyungpook National University, Daegu, South Korea.

⁹Rosenstiel School of Marine and Atmospheric Science, University of Miami, Miami, USA.

¹⁰National Centre for Atmospheric Research, Boulder, Colorado, USA

¹¹Nolan Sherry & Associates, Kingston upon Thames, London, UK.

¹²Laboratory for Air Pollution and Environmental Technology, Empa, Swiss Federal Laboratories for Materials Science and Technology, Duebendorf, Switzerland.

¹³Institute for Atmospheric and Environmental Sciences, Goethe University Frankfurt, Germany.

¹⁴Climate Science Centre, CSIRO Oceans and Atmosphere, Aspendale, Victoria, Australia

¹⁵Department of Pure and Applied Sciences, University of Urbino, Urbino, Italy.

¹⁶National Institute for Environmental Studies, Tsukuba, Japan.

¹⁷School of Chemistry, University of Bristol, Bristol, UK.

¹⁸Norwegian Institute for Air Research, Kjeller, Norway.

[†]Deceased: 19.12.2017

Correspondence to: Tom Claxton (t.claxton@lancaster.ac.uk) or Ryan Hossaini (r.hossaini@lancaster.ac.uk)

Key Points:

- Global dichloromethane emissions increased by ~85% between 2006 and 2017, mostly due to increasing emissions from Asia.
- Perchloroethylene emissions have decreased in the same period, mainly due to reduced emissions from Europe and North America.
- Posterior CH₂Cl₂ and C₂Cl₄ emissions provide good agreement with surface and aircraft observational data.

Abstract

Dichloromethane (CH_2Cl_2) and perchloroethylene (C_2Cl_4) are chlorinated Very Short-Lived Substances (Cl-VSLS) with anthropogenic sources. Recent studies highlight the increasing influence of such compounds, particularly CH_2Cl_2 , on the stratospheric chlorine budget and therefore on ozone depletion. Here, a multi-year global-scale synthesis inversion was performed to optimise CH_2Cl_2 (2006–2017) and C_2Cl_4 (2007–2017) emissions. The approach combines long-term surface observations from global monitoring networks, output from a three-dimensional chemical transport model (TOMCAT), and novel bottom-up information on prior industry emissions. Our posterior results show an increase in global CH_2Cl_2 emissions from $637 \pm 36 \text{ Gg yr}^{-1}$ in 2006 to $1171 \pm 45 \text{ Gg yr}^{-1}$ in 2017, with Asian emissions accounting for 68% and 89% of these totals, respectively. In absolute terms, Asian CH_2Cl_2 emissions increased annually by 51 Gg yr^{-1} over the study period, while European and North American emissions declined, indicating a continental-scale shift in emission distribution since the mid-2000s. For C_2Cl_4 , we estimate a decrease in global emissions from $141 \pm 14 \text{ Gg yr}^{-1}$ in 2007 to $106 \pm 12 \text{ Gg yr}^{-1}$ in 2017. The time-varying posterior emissions offer significant improvements over the prior. Utilising the posterior emissions leads to modelled tropospheric CH_2Cl_2 and C_2Cl_4 abundances and trends in good agreement to those observed (including independent observations to the inversion). A shorter C_2Cl_4 lifetime, from including an uncertain Cl sink, leads to larger global C_2Cl_4 emissions by a factor of ~ 1.5 , which in some places improves model-measurement agreement. The sensitivity of our findings to assumptions in the inversion procedure, including CH_2Cl_2 oceanic emissions, is discussed.

Plain Language Summary

The 1987 Montreal Protocol banned production for dispersive uses of major ozone-depleting gases, such as chlorofluorocarbons, due to their role in depletion of the stratospheric ozone layer. In consequence, the ozone layer is expected to recover in coming decades, as stratospheric chlorine from banned substances slowly declines. However, chlorinated Very Short-Lived Substances (Cl-VSLS), not controlled by the Montreal Protocol, represent a small, but growing, source of atmospheric chlorine that could potentially slow ozone recovery. It is thus important that the magnitude of emissions of these compounds, their spatial distribution, and changes with time are quantified. Here, we combined observations of Cl-VSLS, prior estimates of their emissions, and a chemical transport model to produce an optimised set of emission estimates on a region-by-region basis between 2006 and 2017. We show that industrial emissions of dichloromethane, the most abundant Cl-VSLS, increased by $\sim 84\%$ within this period, predominately due to an increase in Asian emissions, while European and North American emissions decreased. Over 2007–2017, emissions of perchloroethylene, a less abundant Cl-VSLS, decreased, particularly in Europe and North America. We show that our new emission estimates lead to better agreement with observational data compared to previous estimates.

1. Introduction

Halogenated Very Short-Lived Substances (VSLS) are organic compounds with atmospheric lifetimes at the planetary surface of ~ 6 months or less [Engel and Rigby et al., 2018]. These lifetimes are short compared to the principal gases synonymous with ozone depletion, such as chlorofluorocarbons (CFCs), which were banned under the terms of the 1987 Montreal Protocol and its later amendments. However, despite their short lifetimes, over the last two decades a wealth of research has shown that VSLS of both natural and anthropogenic origin can reach the stratosphere, where they contribute to stratospheric bromine and chlorine and thus ozone depletion [e.g. Sturges et al., 2000; Laube et al., 2008; Fernandez et al., 2014; Hossaini et al., 2017; Wales et al., 2018; Claxton et al., 2019]. Brominated VSLS (e.g.

bromoform, dibromomethane) are predominately of natural oceanic origin [e.g. Quack and Wallace, 2003; Ziska et al., 2013], while chlorinated VSLS (Cl-VSLS) have significant anthropogenic sources [e.g. McCulloch et al., 1999; Engel and Rigby et al., 2018]. At present, these compounds account for a small, but growing, portion of atmospheric chlorine and they are not controlled by the Montreal Protocol. In 2016, Cl-VSLS were estimated to provide 115 (75-160) ppt of chlorine to the stratosphere, which represents 3.5% of total chlorine in the stratosphere from all sources [Engel and Rigby et al., 2018; Hossaini et al., 2019].

The most abundant Cl-VSLS, dichloromethane (CH_2Cl_2), is of particular interest owing to an observed rapid increase in its global concentration since the mid-2000s [Leedham Elvidge et al., 2015; Hossaini et al., 2017, 2019]. As a versatile solvent, CH_2Cl_2 has a range of industrial applications and roughly 90% of total emissions have been estimated to be anthropogenic [Montzka et al., 2011]. Annual global CH_2Cl_2 emissions have been estimated at $\sim 1000 \text{ Gg yr}^{-1}$ in 2016, with a global mean surface mole fraction of 33-39 ppt observed from monitoring networks, a factor of ~ 2 larger compared to the early part of the century [Engel and Rigby et al., 2018]. Biogenic CH_2Cl_2 sources have also been hypothesised from the ocean [Ooki and Yokouchi, 2011; Jones and Carpenter, 2005] and from mangrove forests [Kolusu et al., 2018], though the magnitudes of these sources are poorly constrained and are expected to be small. A less abundant Cl-VSLS is perchloroethylene, C_2Cl_4 , which is almost solely anthropogenic and historically has found use for example in dry-cleaning applications. Unlike CH_2Cl_2 , the abundance of C_2Cl_4 has continually decreased over the last few decades [Simpson et al., 2004; Carpenter and Reimann et al., 2014], due to phasing out in favour of less-toxic alternatives. In 2016, the global mean C_2Cl_4 mole fraction was 1.1-1.2 ppt, with global emissions estimated at $83\text{-}103 \text{ Gg yr}^{-1}$ [Engel and Rigby et al., 2018].

Claxton et al. [2019] recently quantified the ozone-depletion potential (ODP) of several Cl-VSLS, highlighting a strong dependence of the ODP on the location of emission. They reported ODP ranges for CH_2Cl_2 and C_2Cl_4 of 0.0097–0.0208 and 0.0057–0.0198, respectively, with emissions from Asia having the largest ODPs. This is significant for Cl-VSLS, as Asian emissions (a) likely account for a large fraction of present-day global total emissions, having grown in importance over the last decade [Leedham Elvidge et al., 2015; Oram et al., 2017; Fang et al., 2019], and (b) may continue to increase in coming years [Feng et al., 2018]. On the above basis, it is important that the geographical distribution and strength of Cl-VSLS emissions are investigated and that accurate, up-to-date inventories are available as input for global modelling studies. Global modelling studies examining the stratospheric input of Cl-VSLS have thus far relied on simple surface mixing ratio boundary conditions to constrain surface abundances of CH_2Cl_2 and other compounds based on measurements in the remote atmosphere. While these are observationally-based and have been implemented so that time trends and latitudinal gradients are captured [Hossaini et al., 2019], zonal variability is not represented by the approach. This includes any potential co-location of elevated emissions with regions of efficient transport pathways to the upper troposphere/stratosphere, such as from continental East Asia [e.g. Ashfold et al., 2015], which are likely relevant to determining accurate ODPs [Claxton et al., 2019].

Despite a growing interest in Cl-VSLS, there have been few recent studies examining their emissions at the global scale. Keene et al. [1999] established the Reactive Chlorine Emissions Inventory (RCEI) framework in which global emissions were estimated using a bottom-up approach for a wide range of chlorocarbons. Within that framework, industrial emissions of 587 Gg yr^{-1} CH_2Cl_2 and 363 Gg yr^{-1} C_2Cl_4 were estimated [McCulloch et al., 1999]. These values, based on analysis relevant to the 1990s, likely underestimate present CH_2Cl_2 emissions and overestimate C_2Cl_4 emissions, based on recent trends [Engel and Rigby et al., 2018]. Khalil

et al. [1999] added to the RCEI framework by estimating total oceanic emissions of 191 Gg yr^{-1} CH_2Cl_2 and 19 Gg yr^{-1} C_2Cl_4 . However, Cl-VSLS fluxes from the ocean are highly spatially variable [e.g. Kolusu et al., 2016] and a significantly lower CH_2Cl_2 source ($<90 \text{ Gg yr}^{-1}$) has been inferred in later work [Trudinger et al., 2004]. Furthermore, while some evidence for in-situ CH_2Cl_2 production (related to biological activity) has been reported [Ooki and Yokouchi, 2011], the ocean may also take up atmospheric CH_2Cl_2 and re-emit it elsewhere [Moore, 2004]. This possibly confounds the interpretation of observational results that were used to infer the magnitude of natural emissions in earlier work. In addition, Lobert [1999] estimated a biomass burning CH_2Cl_2 source of 59 Gg yr^{-1} , though evidence for the existence of this source is missing from more recent analyses [Möhle et al., 2007; Simpson et al., 2011; Lawson et al., 2015; Leedham Elvidge et al., 2015].

There are two core objectives of this study. First, to investigate global and regional changes in CH_2Cl_2 and C_2Cl_4 emission magnitudes and distributions on a multi-annual timescale. Second, to generate and evaluate a set of up-to-date global emissions for both compounds, suitable for use as input to atmospheric models. To accomplish this, we performed a global synthesis inversion to optimise Cl-VSLS emissions over the period 2006-2017. Briefly, this approach combines long-term observations from global monitoring networks, prior information on emissions, and a chemical transport model. The paper is structured as follows. The 3-D chemical transport model is described in Section 2. The inversion procedure is outlined in Section 3, including both the theory and a description of the different observations used. Our main inversion results, including various sensitivity analyses, are presented in Section 4. These include the addition of ocean sources of CH_2Cl_2 , and an added Cl sink of C_2Cl_4 . Conclusions and recommendations for future work are given in Section 5.

2. Description of the TOMCAT Chemical Transport Model

TOMCAT is an offline 3-D Chemistry Transport Model (CTM) [Chipperfield et al., 2006; Monks et al., 2016] that has been widely used to investigate tropospheric chemistry and transport, including several VSLS-focussed studies [e.g. Hossaini et al., 2010, 2019; Claxton et al., 2019]. The CTM is forced by 6-hourly wind, temperature and humidity fields taken from the European Centre for Medium-Range Weather Forecasts (ECMWF) ERA-Interim meteorological reanalyses [Dee et al., 2011]. The TOMCAT configuration used had a horizontal resolution of $2.8^\circ \times 2.8^\circ$, with a vertical resolution of 60 levels, up to an altitude of $\sim 64 \text{ km}$. Our model configuration also employs a simplified tropospheric chemistry scheme, reading an offline monthly-varying field of the tropospheric hydroxyl radical (OH) concentration [Spivakovsky et al., 2000; Huijnen et al., 2010]. The OH field was used in the Atmospheric Tracer Transport Model Intercomparison Project (TransCom) study of CH_4 [Patra et al., 2011], and leads to an average methyl chloroform lifetime (1992-2007) of $4.71 (\pm 0.18)$ years in TOMCAT, in reasonable agreement with recent estimates of ~ 5 years obtained from inverse methods [e.g. Rigby et al., 2013]. Although the model OH field is here fixed in time, we note that evidence for interannual OH variability, for instance due to ENSO activity, exists [e.g. Prinn et al., 2005; Turner et al., 2018].

Both CH_2Cl_2 and C_2Cl_4 are subject to OH oxidation and photolysis sinks in the model. An additional inversion experiment (see ensuing discussion) was performed for C_2Cl_4 in which the competing three-bodied loss reaction of C_2Cl_4 with Cl atoms was also included. The inclusion of this reaction in models has been shown to be important to reproduce atmospheric C_2Cl_4 observations in the upper troposphere [Hossaini et al., 2019]. In this case, the model assumes a fixed tropospheric mean Cl concentration of $1.3 \times 10^3 \text{ atoms cm}^{-3}$ globally, based on model estimates from Hossaini et al. [2016]. In practice, the spatial distribution of tropospheric Cl would be non-uniform and given this uncertainty, this model run is treated as a sensitivity.

Reaction rate constants were taken from the 2015 Jet Propulsion Laboratory (JPL) report [Burkholder et al., 2015]. For the purposes of this study which investigates source gas emissions, product gas chemistry was not required.

3. Description of the Inversion Technique

3.1 Synthesis Inversion

The ‘synthesis inversion’ technique optimises model prior emissions of a given compound by minimising differences between modelled and observed mixing ratios [e.g. Baker et al., 2006]. This top-down technique is well established and has been used to investigate surface emissions of several compounds, including CH₄ [McNorton et al., 2018], CO₂ [Law et al., 2008; Wang et al., 2018], CO [Pétron et al., 2002] and H₂ [Bousquet et al., 2011]. Here, we apply the technique to CH₂Cl₂ and C₂Cl₄ to optimise their emissions for 12-year (2006-2017) and 11-year (2007-2017) periods, respectively, over which a wide range of tropospheric observations are available (Section 3.2). Prior surface CH₂Cl₂ and C₂Cl₄ emissions (Section 3.4) were aggregated over a possible 14 source regions (**Figure 1a**). Boundaries for these source regions (10 land and 4 ocean), which are continental in scale, are adapted from previous TransCom inversion studies [e.g. Baker et al., 2006]. The 4 ocean regions are defined by the following latitude bands: Extratropical Northern Ocean (30-90°N), Tropical Northern Ocean (0-30°N), Tropical Southern Ocean (0-30°S) and Extratropical Southern Ocean (30-90°S). Given the large uncertainty surrounding oceanic CH₂Cl₂ emissions (see discussion in Section 3.2.3), for this compound two different inversions were performed as part of our sensitivity analysis. The first did not include any oceanic CH₂Cl₂ emission (i.e. it assumed industry sources only), while the second also considered emissions from the ocean regions.

Within each source region, the distribution of emission is fixed (see Section 3.4), and the inversion optimises the total emission from each region on an annual basis.

The technique is based on minimising the cost function, J :

$$J(\mathbf{x}) = \frac{1}{2}(\mathbf{x} - \mathbf{x}_b) \cdot \mathbf{B}^{-1} \cdot (\mathbf{x} - \mathbf{x}_b) + \frac{1}{2}(\mathbf{y} - \mathbf{G} \cdot \mathbf{x}) \cdot \mathbf{R}^{-1} \cdot (\mathbf{y} - \mathbf{G} \cdot \mathbf{x}) \quad \text{Equation 1.}$$

where \mathbf{x} is an emission estimate, \mathbf{x}_b are the prior emissions, \mathbf{B} is the covariance matrix for the errors in emissions, \mathbf{y} are the observations, \mathbf{R} is the covariance matrix for the errors in observations, and \mathbf{G} is the normalised model output concentration Jacobian matrix. It maps the emission field on to the observation vector \mathbf{y} via the transport model.

The cost function is at a minimum at $\mathbf{x} = \mathbf{x}_a$, where \mathbf{x}_a is given as [Tarantola and Valette, 1982]:

$$\mathbf{x}_a = \mathbf{x}_b + [\mathbf{G}^T \cdot \mathbf{R}^{-1} \cdot \mathbf{G} + \mathbf{B}^{-1}]^{-1} \cdot \mathbf{G}^T \cdot \mathbf{R}^{-1} \cdot (\mathbf{y} - \mathbf{G} \cdot \mathbf{x}_b) \quad \text{Equation 2.}$$

Since all the other quantities are known, the posterior emissions for each of the 14 regions analysed in the inversion can be solved on a year-by-year basis. Note, our justification for estimating annual emissions (e.g. as opposed to monthly-resolved) is based on several factors that are outlined in Section 3.2.1 below. This solution of \mathbf{x}_a gives the best match to the observations, whilst reducing the likelihood of straying unrealistically from the prior emissions \mathbf{x}_b . A successful inversion is indicated by a significant reduction in errors on the prior emissions relative to the posterior emissions.

3.2 Observations

3.2.1 Surface Observations of CH₂Cl₂ and C₂Cl₄

Most of the CH₂Cl₂ and C₂Cl₄ observational data considered in this study come from remote surface sites, as summarised in **Tables 1** and **2**. We consider monthly mean measurements of both compounds over the 12-year period obtained from a total of 29 unique surface locations, 19 used as input into the inversion, and 10 held back for independent verification. These data are from the National Oceanic and Atmospheric Administration (NOAA) and Advanced Global Atmospheric Gases Experiment (AGAGE) long-term monitoring networks, which have been described extensively in the literature [e.g. Montzka et al., 2018; Prinn et al., 2018]. AGAGE network monthly mean measurements include pollution events, whilst NOAA measurements are filtered for pollution. Observations obtained from the sites in **Table 1** were used directly in the inversion. Between the two networks, a reasonable level of geographical coverage is achieved (see **Figure 1b**). Critically, this includes sites in each of the main industrialised regions where Cl-VSLs emissions are expected to be greatest, such as the continental USA (4 sites), Europe (4 sites) and East Asia (1 site). A conversion factor of 1.1038 was applied to the AGAGE CH₂Cl₂ record to account for a known calibration difference between the NOAA-2003 and AGAGE SIO-14 calibration scales of ~10% [Carpenter and Reimann et al., 2014, Engel and Rigby et al., 2018]. Note, four measurement sites are shared between the two networks; for this study we use both measurements, however we convert AGAGE data to NOAA calibration scales. For C₂Cl₄, NOAA and AGAGE use NOAA-2003 and NOAA-2003B calibration scales respectively, which have been found to agree to within <1%.

Table 1. Summary of Surface Observational Sites Used as Input to the Inversion (Arranged North to South).

Code	Station Name, Location	Lat (°)	Lon (°)	Elevation (m)	Network
ALT	Alert, Canada	82.5	-62.5	190.0	NOAA
ZEP	Zeppelin, Svalbard, Norway	78.9	11.9	490.0	AGAGE
SUM	Summit, Greenland	72.6	-38.4	3209.5	NOAA
BRW	Barrow, AK, USA	71.3	-156.6	11.0	NOAA
MHD	Mace Head, Ireland	53.3	-9.9	5.0	NOAA, AGAGE
JFJ	Jungfraujoch, Switzerland	46.3	8.0	3580.0	AGAGE
LEF	Park Falls, WI, USA	45.9	-90.3	472.0	NOAA
CMN	Monte Cimone, Italy	44.2	10.7	2165.0	AGAGE
HFM	Harvard Forest, MA, USA	42.5	-72.2	340.0	NOAA
THD	Trinidad Head, CA, USA	41.1	-124.2	107.0	NOAA, AGAGE
NWR	Niwot Ridge, CO, USA	40.1	-105.6	3523.0	NOAA
GSN	Gosan, Jeju, South Korea	33.3	126.2	89.0	AGAGE
MLO	Mauna Loa, HI, USA	19.5	-155.6	3397.0	NOAA
KUM	Cape Kumukai, HI, USA	19.5	-154.8	3.0	NOAA
RPB	Ragged Point, Barbados	13.2	-59.5	42.0	AGAGE
SMO	Tutuila, American Samoa	-14.2	-170.6	42.0	NOAA, AGAGE
CGO	Cape Grim, Australia	-40.7	144.7	94.0	NOAA, AGAGE
PSA	Palmer Station, Antarctica	-64.9	-64.0	10.0	NOAA
SPO	South Pole, Antarctica	-90.0	-24.8	2810.0	NOAA

Table 2. Summary of Surface Observational Sites not used as Input in the Inversion. Available in 2015 from the NOAA Tall Tower Network (Arranged North to South).

Code	Station Name, Location	Lat (°)	Lon (°)	Elevation (m)	Network
CRV	CARVE, AK, USA	65.0	-147.6	611.4	NOAA
AMT	Argyle, ME, USA	45.0	-68.7	53.0	NOAA

MBO	Mt. Bachelor, OR, USA	44.0	-121.7	2731.0	NOAA
WBI	West Branch, IA, USA	41.7	-91.4	241.7	NOAA
BAO	Boulder, CO, USA	40.1	-105.0	1584.0	NOAA
WGC	Walnut Grove, CA, USA	38.3	-121.5	0.0	NOAA
STR	Sutro Tower, CA, USA	37.8	-122.5	254.0	NOAA
MWO	Mt. Wilson, CA, USA	34.2	-118.1	1728.0	NOAA
SCT	Beech Island, SC, USA	33.4	-81.8	115.2	NOAA
WKT	Moody, TX, USA	31.3	-97.3	251.0	NOAA

We additionally considered NOAA measurements of both compounds in 2015 from their USA-based tall tower network (**Table 2**). These data were not assimilated in the inversion, but rather were used to provide an independent assessment of the prior versus posterior emissions over the USA (at 10 sites).

The availability and abundance of Cl-VSLS measurement data was a principal factor in our decision to estimate annual mean emissions as opposed to monthly-resolved emissions. The 19 unique observational sites (**Table 1**) provide a maximum of 228 monthly mean measurements in a given year. Solving emissions for 14 different regions would, in a monthly-resolved inversion, require 168 (14×12) model Cl-VSLS tracers for each year of our study period. This number of tracers (168) is comparable to the number of observations we have available to us in a year (maximum of 228 monthly means, assuming no missing data) and would lead to a less well constrained inversion process, as each month's emissions would only be constrained on average by 1.4 observations. In addition, we believe that the large computational expense of running with such a large number of tracers is not warranted on the basis of (1) our study is primarily interested in long-term inter-annual emission trends and (2) the seasonal cycle of Cl-VSLS is found to be reproduced well using our seasonal posterior emissions (see Sections 4.6 and 4.7). Finally, we note that there is little information in the literature with which to inform any prior emission seasonality in our model. However, for CH₂Cl₂ no significant seasonal variation in industrial emissions has been reported [McCulloch and Midgley, 1996]

3.2.2 Aircraft Observations of CH₂Cl₂ and C₂Cl₄

We also considered measurements of both Cl-VSLS from three different flight campaigns: the 2014 Co-ordinated Airborne Studies in the Tropics (CAST) mission [Andrews et al., 2016, Harris et al., 2017], the 2014 Convective Transport of Active Species in the Tropics (CONTRAST) mission [Pan et al., 2017], and the 2014 Airborne Tropical Tropopause Experiment (ATTREX) mission [Navarro et al., 2015]. The locations of these campaigns are shown in **Figure 1b**. The CAST mission (January-February) centred around Guam in the tropical West Pacific and made extensive measurements in the marine boundary layer during 22 flights, with vertical profiles extending up to ~10 km. Likewise, the CONTRAST (January-February) and ATTREX (January-March) missions also sampled the tropical West Pacific in a region centred around Guam. However, these campaigns sampled air from higher altitudes, with ATTREX extending into the lower stratosphere. Data from these three flight campaigns are not used as input to the inversion; instead they are used as independent observations to test the posterior results (in the relevant months of 2014).

3.2.3 Ocean Emission Data

As noted in the Introduction, the ocean is a potential source of CH₂Cl₂ and C₂Cl₄. However, there are large uncertainties and several important confounding issues that require attention.

Given that oceanic emissions have been proposed to be relatively more important for CH_2Cl_2 than C_2Cl_4 [Keene et al., 1999] we focus most of the following discussion on CH_2Cl_2 , which provides a rationale for performing an inversion with and without an ocean CH_2Cl_2 source.

First, there is very limited observational data with which to draw any firm conclusions regarding the strength of any oceanic emission. Khalil et al. [1999] estimated a total oceanic CH_2Cl_2 source of $\sim 196 \text{ Gg yr}^{-1}$ distributed in four latitude bands: $30\text{--}90^\circ \text{N}$ ($\sim 24 \text{ Gg yr}^{-1}$), $0\text{--}30^\circ \text{N}$ ($\sim 50 \text{ Gg yr}^{-1}$), $0\text{--}30^\circ \text{S}$ ($\sim 50 \text{ Gg yr}^{-1}$) and $30\text{--}90^\circ \text{S}$ ($\sim 72 \text{ Gg yr}^{-1}$). Khalil et al. [1999] acknowledged that the data available to them to calculate fluxes, including measured seawater and atmosphere concentrations of CH_2Cl_2 (and C_2Cl_4), were limited. The calculated fluxes were thus deemed to be “extremely uncertain” and later work inferred a significantly smaller upper limit to total ocean CH_2Cl_2 emissions ($< 90 \text{ Gg yr}^{-1}$) based on analysis of firm air samples [Trudinger et al., 2004].

Second, in addition to a paucity of measurements, observational results and expectations suggest the possibility for very large spatiotemporal variability in ocean CH_2Cl_2 fluxes. For example, based on data collected during a cruise in the tropical Atlantic, Kolusu et al. [2016] calculated a mean CH_2Cl_2 flux of $81 (\pm 81.7) \text{ nmol m}^{-2} \text{ day}^{-1}$. Given this large variability, short-term observational studies likely lack sufficient spatial and seasonal coverage to provide adequate estimates of annual net emissions over large domains. Extrapolation to infer regional or global emission totals, while common practice, can be problematic. Extrapolating the Kolusu et al. [2016] flux to a tropical ocean band gives $\sim 236 \text{ Gg yr}^{-1}$; to the entire ocean gives a total of $\sim 915 \text{ Gg yr}^{-1}$. This is a similar order to our prior global emission of $1011.5 \text{ Gg yr}^{-1}$, that includes both land and ocean sources.

Third, another major confounding issue related to the above and relevant to drawing inference on the nature of any ocean CH_2Cl_2 source related to in-situ production, was discussed by Moore [2004]. Due to seasonal changes in CH_2Cl_2 ocean solubility (a decrease in warmer waters) and large seasonal changes in the CH_2Cl_2 concentration, summertime measurements may show ocean supersaturations that are unrelated to in-situ production. In consequence, seasonally-resolved data (or analyses accounting for temporary fluxes arising from physical effects, e.g., Ooki and Yokouchi, [2011]) are needed to determine the degree to which fluxes derived from measured ocean-water saturation are a result of in-situ production or simply seasonal changes in solubility and atmospheric concentration. Moore [2004] also provided strong evidence that dissolved CH_2Cl_2 persists for extended periods (possibly years to decades) in intermediate and deep ocean waters. In consequence, observed CH_2Cl_2 supersaturations in seawater may be caused by its transport from colder waters at higher latitudes. Based on the above, the inferred oceanic CH_2Cl_2 source reported in previous studies [Khalil et al, 1999; Keene et al., 1999] may reflect re-equilibration processes and does not necessarily provide evidence for marine production.

A plausible mechanism by which CH_2Cl_2 may be produced in the ocean has been proposed and involves the photolysis and subsequent reaction of biogenic precursors, such as CH_2ICl , in seawater [Jones and Carpenter, 2005]. To our knowledge, the only observational study that provides some evidence of marine CH_2Cl_2 production (related to phytoplankton) is that of Ooki and Yokouchi [2011]. That study accounted for the physical factors discussed above to derive a marine CH_2Cl_2 in-situ source from the Indian Ocean (between 10°S and 40°S) of $0.29\text{--}0.43 \mu\text{g m}^{-2} \text{ day}^{-1}$. When extrapolated zonally across the globe, a CH_2Cl_2 source of $10\text{--}15 \text{ Gg yr}^{-1}$ was derived for this latitude band. In summary, considering the uncertainties mentioned above, we performed inversions with and without ocean CH_2Cl_2 sources.

For the inversion performed allowing net CH₂Cl₂ emissions from the ocean, we compare posterior emissions from our inversion to novel measurements from two recent ship cruises: (a) AMT-22 (Atlantic Meridional Transect, RRS *James Cook*) and (b) ACCACIA-2 (Aerosol-Cloud Coupling And Climate Interactions in the Arctic, JR288, RRS *James Clark Ross*). These campaigns took place in October/November 2012 and July/August 2013, respectively. AMT-22 covered a track through the Atlantic Ocean from 45°N to 30°S and ACCACIA-2 covered the North Atlantic/Arctic Oceans from 70°N to 80°N, including a navigation around the archipelago of Svalbard, Norway (**Figure 1b**). Along these cruise tracks, sea-to-air flux estimates of CH₂Cl₂ (only) were derived based on in situ automated measurements of CH₂Cl₂ concentrations in surface seawater (from the ships' clean underway seawater supply inlets; nominal depth 5–6 m) and in air from a continuously pumped air inlet [Hackenberg et al., 2017]. Details of the GC-MS measurement systems are given in Andrews et al. [2015]. The CH₂Cl₂ sea-to-air flux was calculated following the approach of Johnson [2010], but would reflect the combination of both physical effects and any in situ production as discussed above. Average fluxes within the latitude limits of our ocean regions (**Figure 1**, Section 3.1) were calculated and an estimate of the global ocean emission from each latitude band was obtained through a simple extrapolation. These integrated fluxes are a starting point to compare to our posterior ocean emissions for CH₂Cl₂ in Section 4.4.

3.3 Observation Errors

The covariance matrix for errors in observations (e.g. **R** in **Equation 1**) is made up of various error sources. Our approach to quantifying these follows the framework described by Xiao [2008], which considers (1) 'sampling frequency' errors, (2) 'measurement' errors and (3) 'mismatch' errors [Chen and Prinn, 2006]. Each of these terms are used to define the total observational error and are detailed in turn below.

3.3.1 Sampling Frequency

The first error source arises due to the sampling frequency of the observational networks. That is, how well the observed monthly mean CH₂Cl₂ or C₂Cl₄ mole fractions are described by a finite number of measurements [Xiao, 2008]. For each site, and each month, the total sampling frequency error, σ_{sf} , for an observational point is given as:

$$\sigma_{sf} = \sqrt{\frac{\sigma_{mon}^2}{m}} \quad \text{Equation 3.}$$

where σ_{mon}^2 is the variance of the reported mole fractions over the month, and m is the number of observations in that month. For AGAGE surface sites, where measurements are obtained at relatively high frequency (order of 200 measurements per month), the sampling frequency error is calculated according to **Equation 3**. As it is difficult to assess the independence of successive measurements, **Equation 3** assumes uncorrelated observations. This might lead to an underestimation in σ_{sf} , but this is likely to be small compared to the overall error. For the NOAA surface sites, mole fractions are obtained based on paired flask samples obtained approximately weekly (i.e. relatively low frequency). Therefore, following Xiao [2008] sampling frequency errors for the NOAA data points were generated from the TOMCAT model, using 30-minute averaged output at each of the NOAA locations.

3.3.2 Measurement Error

A second source of error arises from errors in the measurements. These can result from instrument precision or other uncertainties in the measuring techniques, such as calibration imperfections. Every observation will have a measurement error, although these are often

difficult to fully estimate. In terms of precisions, the AGAGE network reports 0.5% for both CH₂Cl₂ and C₂Cl₄ based on the measurement precisions of the working standard used [Prinn et al., 2018], whilst the NOAA network reports precision for each individual measurement, which is aggregated over each month (typically around 0.7%). In this study, we assume a minimum overall 5% measurement error (σ_{meas}) for both compounds. This value is based on the study of Andrews et al. [2016] who performed an intercomparison of CH₂Cl₂ mole fractions obtained by four different instruments, operated by four different groups, using the same standards. The results indicated that the mean absolute percentage error between the four instruments was ~5% in the troposphere.

3.3.3 Mismatch Error

An additional source of error is the mismatch between the observations and the model. This arises when comparing relatively low spatial resolution model output to point observations. An observational site could be unrepresentative of the model grid cell that it is located in. For example, the Harvard Forest (HFM) surface site is in the same TOMCAT grid cell as New York and other parts of the US Eastern seaboard. However, the site lies in the middle of a forest with presumably lower emissions, and concentrations more characteristic of other rural observations. To take this into account, a mismatch error can be defined using the neighbouring grid cells [Chen and Prinn, 2006]. This is defined in **Equation 4**:

$$\sigma_{\text{mismatch}} = \sqrt{\frac{1}{9} \sum_{i=1}^9 (c_i - \bar{c})^2} \quad \text{Equation 4.}$$

where c_i is the model concentration output for each of the eight neighbouring grid cells, taken as an annual mean, and \bar{c} is the mean model output over the nine cells. The mismatch error equation is a measure of the spatial variance, and although is not a perfect metric it helps to place uncertainty on observations with significant variation in their locality.

The three sources of error are combined in **Equation 5** to give a total observational error:

$$\sigma_{\text{total}} = \sqrt{\sigma_{\text{sf}}^2 + \sigma_{\text{meas}}^2 + \sigma_{\text{mismatch}}^2} \quad \text{Equation 5.}$$

Of the three error terms contributing in **Equation 5**, the sampling frequency term is typically small (<0.1% relative to observations) compared to, for example, the measurement error (5%). The size of the mismatch error is on average 2%, but can vary strongly across sites. For some sites, particularly ones that neighbour urban locations, it can be as large as 15%, or even up to 150% at one site in particular (GSN). For more remote sites (e.g. in the Arctic) the mismatch error could be as low as 0.5%, ten times lower than the measurement error.

3.4 Prior Emissions: Magnitude and Errors

Our prior emission estimates for CH₂Cl₂ and C₂Cl₄ are summarised in **Tables 3** and **4**, respectively. Note that these annual priors are held constant over each year of the inversion period. For CH₂Cl₂, prior estimates of Asian, European and North American emissions (i.e. the expected 3 most significant industrialised regions) are 671, 50, and 55 Gg yr⁻¹ respectively (Nolan Sherry Associates, NSA). These bottom-up estimates (see also **Table S1**), were commissioned for this study and represent expected industrial emissions in 2016, based on a global industry database of chloromethane production and production capacity available to NSA. Production figures are calculated and refined by a combination of this extensive database, industry dialogue, trade data, and back-calculations based on known feedstock applications and quantities. These are entered into a chloromethanes mass balance scheme which is checked against industry capacity and closely calculated production ratios. Of the 671 Gg yr⁻¹ industry

estimate of total Asian CH_2Cl_2 emissions from NSA, 621 Gg yr^{-1} (~93%) is set as the inversion prior estimate for our Temperate Asia region (incorporating the NSA data for China, India, Japan and Korea). The remaining 50 Gg yr^{-1} is taken as the prior for our Tropical Asian region (where NSA analysis shows the major markets for CH_2Cl_2 are Thailand, Indonesia, Singapore, Malaysia, and Vietnam). For the other six land regions, in the absence of more recent up-to-date data, prior industry CH_2Cl_2 emissions are taken from the RCEI, as summarised by Keene et al. [1999].

Recall, for CH_2Cl_2 two inversions are performed, one without ocean emissions and one with. For the without ocean case, our global total CH_2Cl_2 prior is $\sim 815 \text{ Gg yr}^{-1}$ (**Table 3**); i.e. considering industrial emissions only. For the with ocean case, prior estimates of ocean CH_2Cl_2 emissions from 4 different ocean regions (see also Sections 3.1 and 3.2) are taken from Khalil et al. [1999], also part of the RCEI framework. The total ocean CH_2Cl_2 prior is 197 Gg yr^{-1} , increasing the global total prior to 1012 Gg yr^{-1} in the ‘with ocean’ inversion case (**Table S2**). Note, the original RCEI inventory also included a small biomass burning CH_2Cl_2 source of 59 Gg yr^{-1} [Lobert et al., 1999]. However, this estimate was based on an assumed single global $\text{CH}_2\text{Cl}_2/\text{CO}$ emission ratio for all fuel types. Subsequent studies have reported a lower (by two orders of magnitude) $\text{CH}_2\text{Cl}_2/\text{CO}$ ratio [Simmonds et al., 2006] or have found no evidence for significant CH_2Cl_2 enhancements in biomass burning plumes [Möhle et al., 2007; Simpson et al., 2011; Lawson et al., 2015; Leedham Elvidge et al., 2015]. On this basis, a biomass burning CH_2Cl_2 source was not considered in the present work.

For C_2Cl_4 , a similar approach was adopted whereby prior industry emission estimates for our Asia, Europe and North American regions, are based on 2016 bottom-up estimates obtained from NSA (**Table 4**, **Table S1**). Similarly to CH_2Cl_2 , the Asia estimate is distributed among our Temperate and Tropical Asian regions as 93.3 and 15.0 Gg yr^{-1} , respectively. For the other six land regions, prior C_2Cl_4 emissions were formulated by reducing industrial emissions from the RCEI inventory by a factor of 2. This reduction was performed because tropospheric C_2Cl_4 mixing ratios have been observed to be declining since 2000 or earlier [e.g. Simpson et al., 2004; Simmonds et al., 2006], meaning the older RCEI estimates (formulated in the 1990s) are very likely to overestimate present-day emissions. The magnitude of our resultant global total C_2Cl_4 prior emission (207 Gg yr^{-1}), of which 9% is from the ocean, is therefore in closer agreement to more recent independent global estimates [e.g. Engel and Rigby et al., 2018].

In addition to the observational errors necessary to the inversion procedure (Section 3.3), there are also errors in the prior emission estimates discussed above. As these are generally poorly quantified in inversion studies, they are set to $\pm 100\%$ for all regions as default. The sensitivity of our results to assumptions about prior errors is discussed in Section 4.3.

3.5 Prior Emissions: Distribution

Within the continental-scale regions considered in this study (**Figure 1a**), CH_2Cl_2 emissions are distributed according to a recent $1^\circ \times 1^\circ$ global HCFC-22 emissions inventory reported by Xiang et al. [2014]. The rationale behind this choice is that CH_2Cl_2 is co-produced by industry with CHCl_3 [Zhang et al., 2015], and the latter is used almost exclusively as a feedstock in the production of HCFC-22 and fluoropolymers [Tsai, 2017; Fang et al., 2018; Möhle et al., 2019], despite CH_2Cl_2 emissions likely being primarily associated with use, not production. On this basis, use of the HCFC-22 emission distribution can be used as a reasonable proxy for CH_2Cl_2 , and is a desirable alternative to the far older RCEI distribution. We understand that HCFC-22 is also likely to be emitted where it is used, not where it is produced, which makes this a rough approximation. In the similar absence of more recent data, the HCFC-22 distribution was used as a proxy for C_2Cl_4 . It is important to stress that (a) these distributions only affect fluxes within

regions (**Figure 1a**) and (b) that the inversion procedure adjusts the integrated regional total emissions, on a region-by-region basis. The distribution of our prior CH₂Cl₂ emissions is presented in **Figure S1**. It is assumed that the within-region distribution does not change over our study period (2006-2017).

4. Results and Discussion

4.1 Posterior CH₂Cl₂ Emissions and Trends

The synthesis inversion produces regional emission estimates, on an annual basis, for each of the 12 years studied. We investigated the degree to which our inversion was able to differentiate between emissions arising from one region over another. A strong negative covariance was found for the closely located regions, Temperate Asia and Tropical Asia, which implies a difficulty in differentiating between these two regions. On this basis, in the ensuing discussion results from these regions are combined and referred to as “combined Asia”. We first consider results from the “no ocean” CH₂Cl₂ inversion. **Table 3** compares prior and posterior CH₂Cl₂ emissions for 2006 and 2017, the first and last years of our study, highlighting an increase in posterior global total CH₂Cl₂ emissions from 637 ± 37 Gg yr⁻¹ (2006) to 1171 ± 45 Gg yr⁻¹ (2017). This 84% increase is largely due to increasing emissions from combined Asia, estimated to rise from 431 ± 32 Gg yr⁻¹ in 2006 to 1045 ± 40 Gg yr⁻¹ in 2017. Our results thus imply that combined Asian emissions more than doubled during the study period and account for ~70% of global total CH₂Cl₂ emissions in 2006 and ~90% in 2017. The latter is a similar relative proportion to that derived from the bottom-up information from NSA presented in **Table S1**.

Table 3. A Summary of Prior (2016 Best Estimate) and Posterior CH₂Cl₂ Emissions (Gg yr⁻¹) and their Uncertainties, from the Synthesis Inversion.

Region	Prior Emissions	2006		2017	
		Posterior Emissions	Error Reduction	Posterior Emissions	Error Reduction
Europe	50.0	112.0 ± 9.1	81.9%	75.1 ± 11.4	77.3%
Africa	9.18	16.6 ± 8.4	8.0%	19.2 ± 8.7	5.2%
Australia	4.85	3.90 ± 2.22	54.2%	3.41 ± 2.62	45.9%
Boreal Asia	6.81	-19.8 ± 5.4	20.5%	-21.8 ± 6.2	9.3%
Boreal NA	1.11	0.002 ± 1.08	3.0%	0.14 ± 1.11	1.1%
Temperate Asia	621.0	89.9 ± 22.8	96.3%	590.7 ± 28.4	95.4%
Temperate LA	8.43	-2.57 ± 4.68	44.5%	0.96 ± 5.62	33.4%
Temperate NA	55.0	71.1 ± 4.9	91.1%	32.1 ± 5.9	89.3%
Tropical Asia	50.0	341.4 ± 22.7	54.5%	454.2 ± 28.7	42.6%
Tropical LA	8.67	24.1 ± 7.8	10.1%	17.1 ± 8.1	7.0%
Combined Asia	671.0	431.3 ± 32.2	-	1044.9 ± 40.4	-
Global Total	815.1	636.6 ± 36.5	-	1171.2 ± 44.9	-

Note. See the main text for a description of the prior emissions. NA = North America, LA = Latin America. Combined Asia = Temperate + Tropical.

While there are no other estimates of *total* Asian CH₂Cl₂ emissions in the literature, to our knowledge, some country-specific estimates have been reported. Oram et al. [2017] roughly estimated Chinese CH₂Cl₂ emissions of 455 (410-500) Gg yr⁻¹ in 2015 from bottom-up information from NSA. However, significantly smaller Chinese CH₂Cl₂ emissions in 2016 of 318 (254–384) Gg yr⁻¹ have also been reported, apparently also based on bottom-up information [Feng et al., 2018], thus highlighting the uncertainty in the regional budget. Our

estimate of total Asian emissions (1045 Gg yr^{-1} in 2017) includes emissions from other major economies, such as India, expected to be significant emitters of CH_2Cl_2 [e.g. Leedham Elvidge et al., 2015]. The sensitivity of the above findings to inclusion of ocean emissions in our inversion is discussed in Section 4.4.

For other major industrialised regions, North America and Europe, our posterior emissions show a decrease over the 12-year study period (2006-2017). CH_2Cl_2 emissions from North America decreased from 71 ± 5 to $32 \pm 6 \text{ Gg yr}^{-1}$ (-55%) and from Europe decreased from 112 ± 9 to $75 \pm 11 \text{ Gg yr}^{-1}$ (-33%). Again, there is limited information in the literature to compare these findings to. Combining surface observations, model calculations, and CO ratio methods, Simmonds et al. [2006] derived European top-down CH_2Cl_2 emissions of 51-61 Gg yr^{-1} over the 2002-2004 period. Our estimate of European CH_2Cl_2 emissions, for the closest year to their study (2006), is larger at 112 Gg yr^{-1} . Simmonds et al. [2006] also reported a bottom-up estimate of industrial CH_2Cl_2 emissions of 139 Gg yr^{-1} from Europe, based on industry sales, in 2002/03. We note that this is a very similar figure to our bottom-up estimate from NSA (albeit for 2007, **Table S1**).

Figure 2 presents a time series of annual posterior CH_2Cl_2 emissions for a selection of the most important regions. The top panel shows the global total CH_2Cl_2 emission over the 12-year study period, the middle panel the contribution from our combined Asian region, and the bottom panel European and North American emissions. Also shown in the top panel are independent estimates of global CH_2Cl_2 emissions (2006-2016 only) calculated from a 12-box model forced by either NOAA or AGAGE long-term surface measurements [e.g. Rigby et al., 2013, Cunnold et al., 1983]. These annual emission data were prepared for the 2018 WMO/UNEP Scientific Assessment of Ozone Depletion and show CH_2Cl_2 emissions increasing from $442\text{-}759 \text{ Gg yr}^{-1}$ in 2006 to $698\text{-}1256 \text{ Gg yr}^{-1}$ in 2016, with the ranges in each period reflecting results obtained considering the two different observational networks analysed by the 12-box model [Engel and Rigby et al., 2018]. Good agreement between results from this study and those of the 12-box model is found, particularly when the latter assimilates NOAA data, which is plausible as our model also incorporates CH_2Cl_2 data on the NOAA calibration scale. For example, our global total CH_2Cl_2 emission in 2006 ($637 \pm 37 \text{ Gg yr}^{-1}$) and 2016 ($1117 \pm 41 \text{ Gg yr}^{-1}$) fall within the 12-box model ranges noted above. In the most recent years, our posterior emissions fall towards the upper bound of the full uncertainty range of the 12-box model calculations (**Figure 2**). The relative increase in global CH_2Cl_2 emissions between 2006 and 2016 is 61% (12-box model average) and 75% (this work), and the mean annual differences (± 1 s.d.) between our total emissions and the 12-box model AGAGE and NOAA estimates are $159 \pm 51 \text{ Gg yr}^{-1}$ and $42 \pm 36 \text{ Gg yr}^{-1}$, respectively.

Our inversion approach allows us to examine the regional drivers of the increase in global CH_2Cl_2 emissions, which – as apparent from **Figure 2b** – are strongly driven by increasing emissions from Asia. In contrast, the relative changes in emissions from Europe and North America over the study period are relatively small. As previously noted, both these regions see an overall decrease in emissions, though the time series is also characterised by significant inter-annual variability (**Figure 2c**). **Figure 2** also includes, on a regional basis, the bottom-up estimates of CH_2Cl_2 emissions from NSA for Asia, Europe and North America in the years 2007 and 2016 (**Table S1**). Recall, these 2016 inventory-based estimates were used as the prior emissions for these three respective regions in our inversion (see Section 3.4). Like top-down estimates, any bottom-up inventory-based emission data is subject to uncertainty. Therefore, we do not over interpret these data, though note that (a) they imply a striking decrease in European CH_2Cl_2 emissions between 2007 and 2016 that is larger than predicted by our posterior emissions, and (b) that discrepancies between top-down CH_2Cl_2 emissions (from

Europe) and bottom-up estimates have been previously reported [Simmonds et al., 2006]. Our North American posterior emissions in 2007 more closely relate to the bottom-up estimate, however our posterior emissions in 2016 are slightly lower than the bottom-up estimate, but agree within the uncertainty range of the inversion (**Figure 2c**).

4.2 Posterior C₂Cl₄ Emissions and Trends

The posterior C₂Cl₄ emissions are summarised in **Table 4** and **Figure 3**. The tabulated results are based on an inversion that only included loss of C₂Cl₄ by OH and photolysis, ignoring the C₂Cl₄ + Cl sink. Correlations between regions were analysed in the same manner as for CH₂Cl₂, and a strong negative covariance was found between the Temperate and Tropical Asia regions. Therefore, we also employ the same “Combined Asia” for the ensuing discussion. Based on this inversion set up, global total C₂Cl₄ emissions decreased from 141 ± 14 Gg yr⁻¹ in 2007 to 106 ± 12 Gg yr⁻¹ in 2017. Both are significant reductions compared to our prior estimate of 207 Gg yr⁻¹. Also shown in **Figure 3** are (a) emission estimates prepared using a 12-box model as reported by Engel and Rigby et al. [2018], and (b) regional bottom-up estimates of C₂Cl₄ emissions commissioned for this work (**Table S1**). The 12-box model results show global C₂Cl₄ emissions decreasing from 95-199 Gg yr⁻¹ in 2007 to 66-160 Gg yr⁻¹ in 2016. The ranges in these values reflect the two different observational datasets used to force the model. Our posterior emissions show similar absolute decreases, from 141 ± 14 Gg yr⁻¹ to 104 ± 10 Gg yr⁻¹ over the same period. Similarly, the relative decrease in global C₂Cl₄ emissions (2007-2016) is 24% (12-box model average) and 26% (this work), and the mean annual differences (± 1 s.d.) between our total emissions and the 12-box model AGAGE and NOAA estimates are 26 ± 6 Gg yr⁻¹ and 13 ± 7 Gg yr⁻¹, respectively.

As described above, there is very good agreement between global C₂Cl₄ emissions derived in this work and those from Engel and Rigby et al. [2018], which used primarily the same observations, though analysed with a simpler (12-box) model. However, there are clear

Table 4. A Summary of Prior (2016 Best Estimate) and Posterior C₂Cl₄ Emissions (Gg yr⁻¹) and their Uncertainties, from the Synthesis Inversion.

Region	Prior Emissions	2007		2017	
		Posterior Emissions	Error Reduction	Posterior Emissions	Error Reduction
Europe	48.0	65.2 ± 4.4	90.9%	36.6 ± 2.6	94.6%
Africa	2.30	3.77 ± 2.20	4.5%	3.65 ± 2.09	9.2%
Australia	0.62	1.44 ± 0.33	47.1%	0.52 ± 0.25	59.7%
Boreal Asia	1.80	-2.34 ± 1.66	7.6%	-2.69 ± 1.60	10.9%
Boreal NA	0.50	-0.06 ± 0.48	5.3%	0.52 ± 0.47	6.7%
Temperate Asia	93.3	1.92 ± 8.80	90.6%	6.47 ± 7.35	92.1%
Temperate LA	1.06	2.00 ± 1.03	2.8%	2.04 ± 0.97	9.1%
Temperate NA	24.0	44.8 ± 2.7	88.6%	33.5 ± 1.8	92.3%
Tropical Asia	15.0	38.1 ± 8.0	45.1%	35.0 ± 7.9	46.1%
Tropical LA	1.58	2.73 ± 1.55	2.1%	2.29 ± 1.53	3.3%
Extratropical NO	3.51	-16.5 ± 2.2	37.8%	-12.6 ± 1.7	51.2%
Extratropical SO	5.85	-0.50 ± 0.79	86.4%	-0.14 ± 0.65	89.0%
Tropical NO	3.51	-0.63 ± 1.66	52.7%	1.06 ± 1.59	54.5%
Tropical SO	5.85	0.93 ± 1.25	78.7%	-0.09 ± 1.25	78.7%
Combined Asia	108.3	40.0 ± 11.9	-	41.4 ± 10.8	-
Global Total	206.5	140.8 ± 13.8	-	106.1 ± 12.0	-

Note. Results are based on inversion that did not include the C₂Cl₄ + Cl sink.

discrepancies between our regional posterior emissions and the regional bottom-up estimates from NSA shown in **Figure 3**. First, our posterior results for Europe show declining emissions over the study period. While a decline is consistent with the bottom-up data, the magnitude of emissions is not in agreement, with the inversion showing lower C₂Cl₄ emissions in both 2007 and 2016 (in 2016 by a factor of ~2.2 lower). Second, our inversion produces far lower Asian emissions than implied from the bottom-up data. The latter show an increase in Asian C₂Cl₄ emissions from 66 Gg yr⁻¹ in 2007 to 108 Gg yr⁻¹ in 2016. For comparison, our posterior combined Asian emissions in the same years are 40 ± 12 Gg yr⁻¹ and 41 ± 9 Gg yr⁻¹, respectively. The bottom-up Asian 2016 estimate (108 Gg yr⁻¹) is larger than the 2016 global total emissions calculated from both our inversion, and from the average of the 12-box model estimates [Engel and Rigby et al., 2018]. Better agreement is found for North American emissions (**Figure 3**).

Unlike for CH₂Cl₂, tropospheric loss of C₂Cl₄ via Cl radicals (in addition to OH oxidation) can be a significant sink, although its magnitude is not well constrained as the concentration of tropospheric Cl radicals is uncertain. Its inclusion in global models has been shown to lead to better agreement with C₂Cl₄ observations, particularly in the upper troposphere [e.g. Hossaini et al., 2019]. The main inversion results discussed above did not consider this sink, nor did the 12-box model estimates [Engel and Rigby et al., 2018]. A second inversion was performed that did include this additional C₂Cl₄ sink. The posterior results from that inversion are presented in **Table S3** and shown with dashed lines in **Figure 3**. It is evident that inclusion of the Cl atom sink for C₂Cl₄ significantly changes the predicted global total C₂Cl₄ emissions. As would be expected, emissions are larger in the presence of an additional atmospheric loss process. For example, we estimate global total C₂Cl₄ emissions of 106 ± 12 Gg yr⁻¹ in 2017 without the Cl sink (**Table 4**), and 162 ± 12 Gg yr⁻¹ with it (**Table S3**, i.e. 53% larger). On a regional basis, Asian emissions provide the bulk of this increase, with 90% larger combined Asian C₂Cl₄ in 2017 when the C₂Cl₄ + Cl sink is included compared to without it. Inclusion of the sink reduces the discrepancy between our posterior Asian emissions and the NSA bottom-up estimates (**Figure 3b**), though our emissions are still lower in the present day. Better agreement is also obtained for Europe, while North American emissions are broadly unchanged. It is expected that agreement between our posterior C₂Cl₄ emissions and the 12-box model are poorer in absolute magnitude when the Cl sink is included, as this sink is absent in the 12-box model study. However, we note that the trends remain similar.

4.3 Posterior Errors

Our inversion procedure calculates the error in the posterior emissions from the terms in **Equation 1**, using the relationship in **Equation 6**:

$$\text{Posterior error matrix, } \mathbf{A} = [\mathbf{G}^T \cdot \mathbf{R}^{-1} \cdot \mathbf{G} + \mathbf{B}^{-1}]^{-1} \quad \text{Equation 6.}$$

To find the regional emission error, the square root of the leading diagonal elements of **A** are taken. **Tables 3** and **4** show the regional posterior errors for CH₂Cl₂ and C₂Cl₄, respectively. The percentage reductions between the prior error and the posterior errors are also given in these tables. A large error reduction implies more confidence in the posterior solution, and for CH₂Cl₂ the largest reductions occur for the main emitting regions where observations are available; e.g. Temperate North America (89% error reduction for CH₂Cl₂ in 2017), Temperate Asia (95%) and Europe (77%). Note, these values should be considered in tandem with the posterior errors themselves. For example, although Europe has a significant error reduction (e.g. in 2017 a reduction of 77%), this results in a posterior error of ±11 Gg yr⁻¹, which is a

15% of the actual posterior CH₂Cl₂ emission from this region. The inverse is true for Temperate Asia, where relatively large posterior emissions (591 Gg yr⁻¹ in 2017) and a large error reduction (95%) lead to a very small (5%) error in the posterior emission. The C₂Cl₄ errors generally show a similar behaviour, with the largest prior versus posterior error reduction achieved for the main industrial regions where large emissions are derived.

A small error reduction corollary is a sign of less confidence in the posterior emissions. For both compounds, these generally apply to regions that are minimally constrained by local observations, such as Africa and tropical Latin America. Fortunately, as it is assumed that these regions do not contribute much to the total global emissions, relatively large uncertainty in their regional posterior emissions have minimal impact on our findings. That said, we highlight Boreal Asia, a region that is a small net source in our prior emissions (6.8 Gg yr⁻¹ for CH₂Cl₂, 1.8 Gg yr⁻¹ for C₂Cl₄) but becomes a net sink for both compounds in our posterior solution. In 2017, our posterior emissions for Boreal Asia are -22 (±6) Gg yr⁻¹ for CH₂Cl₂ and -2.7 (±1.6) Gg yr⁻¹ for C₂Cl₄. For this region, the percentage reductions between the prior error and the posterior error is small (**Tables 3-4**). While some chlorocarbons are taken up by terrestrial ecosystems [e.g. Khalil and Rasmussen, 1999], no terrestrial sinks of CH₂Cl₂ have been reported, and the lack of observational constraints in this region could point towards a small inversion artefact. An analysis of covariances did not reveal a strong coupling between Boreal Asia and another region.

4.4 Ocean Emissions

Thus far we have largely focussed on our posterior emissions from land (in the “no ocean” inversion for CH₂Cl₂). In this section, we examine ocean emissions. A summary of posterior CH₂Cl₂ emissions with the ocean source included is given in **Table S2** and can be compared to the equivalent no ocean case (**Table 3**). In the inversion in which net emissions from the ocean are allowed, oceanic CH₂Cl₂ emissions (sum from all 4 ocean bands) account for 197 Gg yr⁻¹ (19%) of our prior global total emission, decreasing to 162 Gg yr⁻¹ (14%) in our posterior solution in 2017. The global total CH₂Cl₂ emission is relatively insensitive to the inclusion of the ocean source, 1171 ± 45 Gg yr⁻¹ (no ocean) versus 1166 ± 64 Gg yr⁻¹ (with ocean) for 2017. However, inclusion of the ocean decreases the combined Asia posterior emissions by ~18%, from 1045 ± 40 Gg yr⁻¹ (no ocean) in 2017 to 886 ± 53 Gg yr⁻¹ (with ocean). This effect is largely explained by the inversion placing emissions of CH₂Cl₂ in the tropical Northern Ocean (0-30°N latitude). As was the case in the “no ocean” inversion, **Figure S2** highlights increasing Asian emissions over our study period, while European and North American emission decrease. With the ocean included, the Combined Asian emissions provide a closer match to the bottom-up NSA estimates of industrial Asian emissions (i.e. our prior) in 2016 (**Figure S2**). However as mentioned later in Section 4.6, there is no discernible difference in performance between the two inversions when comparing with observations (even independent data), despite these changes in Asian emissions.

The geographical distribution of our posterior ocean CH₂Cl₂ emissions differs significantly from the prior in the inversion that allows non-zero ocean fluxes. For example, when averaged over the entire 12-year study period, the Extratropical Northern Ocean represents a net sink of CH₂Cl₂ (**Table 5**). In the extratropical Southern Ocean, the derived net flux is significantly lower than the prior but remains positive. Also shown in **Table 5** are results from the inversion study of AGAGE and NOAA observations by Xiao [2008], who allowed non-zero fluxes from the ocean and tabulated ocean CH₂Cl₂ emissions from these same latitude bands. Posterior emissions for the Tropical Northern and Extratropical Southern Oceans from our study fall within the Xiao [2008] uncertainty ranges. However, notably the significant mean CH₂Cl₂ sink we derive to the Extratropical Northern Ocean is not apparent in the Xiao [2008] study for the

observations during 2000-2005, a period before the large atmospheric increase in CH_2Cl_2 occurred.

Table 5. CH_2Cl_2 Ocean Emissions for this Inversion, a Previous Inversion, and for Four Observational Studies.

Ocean band	This work ^a	Xiao [2008] ^b	AMT-22 Campaign ^c	ACCACIA-2 Campaign ^c	Kolusu et al. [2016] ^c	Ooki and Yokouchi [2011] ^d
Extratropical NO	-64.4 ± 10.9	3.5 ± 3.0	14.7 ± 26.9	-47.9 ± 32.7		
Tropical NO	111.8 ± 43.1	88 ± 29	70.9 ± 63.6		236 ± 237	
Tropical SO	9.9 ± 12.7	31 ± 24	64.0 ± 43.3			12.5 ± 2.5
Extratropical SO	4.3 ± 3.9	2 ± 5				

Note. All measurements converted into Gg yr^{-1} . Reported uncertainties for inversion calculations and campaign ocean tracks of 1 std dev. NO = Northern Ocean, SO = Southern Ocean. ^a12-year average posterior emission; ^b5-year average posterior emission from 2000-2005; ^cAtlantic Ocean sea-to-air flux measurements, originally reported as $\text{nmol m}^{-2} \text{day}^{-1}$, and converted into $\text{Gg band}^{-1} \text{yr}^{-1}$ for the relevant ocean latitude bands. AMT-22 campaign measurements took place in Oct-Nov 2012, ACCACIA-2 campaign measurements in July-Aug 2013, and Kolusu et al. [2016] measurements in Apr-May 2009; ^dIndian Ocean biogenic production from phytoplankton, reported between 10°S and 40°S in $\mu\text{g m}^{-2} \text{day}^{-1}$. These measurements were taken from Nov 2009-Jan 2010, and account for physical effects that are the likely principle source in the sea-to-air flux measurements.

It is also possible to perform a basic comparison of our posterior ocean CH_2Cl_2 emissions to observed estimates based on (limited) cruise data. As noted in Section 3.2.3, ocean CH_2Cl_2 sea-to-air fluxes from the AMT-22 and ACCACIA-2 ship cruises (see tracks in **Figure 1b**) were derived based on concentration measurements without consideration of the potential influence of physical effects on the derived fluxes. These cruises sampled in three out of the four ocean bands used in our inversion and the integrated flux from each ocean band is presented in **Table 5**. Broadly, the sign of the emissions agrees in all three regions observed, however it is important to note that this comparison is potentially confounded by considering annual average inversion results to cruise data that we expect could be influenced by seasonally-varying sea-to-air fluxes based on seasonal changes in solubility and atmospheric concentrations [Moore, 2004].

Xiao [2008] reports a large seasonal cycle in ocean emissions, and for the $30\text{-}90^\circ\text{N}$ region there is a maximum of approximately 20 Gg yr^{-1} in the summer, and a minimum of -10 Gg yr^{-1} in the winter. We note that ACCACIA-2 took place during July-August, and reported an average flux of -48 Gg yr^{-1} , which is contrary to what the seasonal cycle states. However, neither our inversion nor that of Xiao [2008] can resolve only between $60\text{-}80^\circ\text{N}$, where ACCACIA-2 took place. AMT-22, measuring from $30\text{-}50^\circ\text{N}$ in autumn, calculates an average flux of 15 Gg yr^{-1} , which is close to the average autumnal values from Xiao [2008]. In the original RCEI estimates, none of the ocean tracks used to infer CH_2Cl_2 fluxes took place above 60°N [Khalil et al, 1999], therefore the large summer sink observed by ACCACIA-2 at these very high latitudes could be evidence for the significant interregional variation we see in our inversion results.

Also presented in **Table 5** is an estimate of an ocean CH_2Cl_2 source based on measurements in the tropical Atlantic from April to May in 2009 [Kolusu et al., 2016]. This source is very uncertain and is generally much higher than any single ocean band emission derived from the inversion. As with the cruises previously discussed, these data do not necessarily support marine CH_2Cl_2 production because of the strong potential for changes in sea-to-air flux related to seasonality in solubility and atmospheric concentrations. Rather, this data simply highlights an ocean region where a significant quantity of CH_2Cl_2 may enter the atmosphere (at least during the period of the campaign of April-May). Due to the large uncertainty it is difficult to say how representative the observations are, as the study showed there was a strong latitudinal gradient, especially when crossing the Equator [Kolusu et al., 2016]. Lastly in **Table 5** are estimated biogenic CH_2Cl_2 emissions reported by Ooki and Yokouchi [2011] based on data collected in the tropical Southern Indian Ocean (10-40° S). Factoring in the uncertainty ranges, our inversion emissions from the tropical Southern Ocean are comparable.

In summary, our posterior CH_2Cl_2 net ocean source (11% of the global total from all sources in 2017, or 125 Gg yr⁻¹) is comparable to previous inversion estimates and to a small set of available oceanic observations. However, whilst the total source magnitude is comparable, the distribution shifts the majority of the emissions into the Tropical NO region, and very few emissions into the Tropical SO region. This distribution is likely a consequence of the large driving force of Combined Asian land emissions; practically it is plausible that the tropical distribution is more even, as observations suggest. For C_2Cl_4 , the posterior ocean source is negligible, and often negative (**Table 4**). For both compounds, our inversion does not distinguish between ocean re-emission and, if it exists, ‘true’ marine production.

4.5 Sensitivity to Prior Uncertainty

Our prior emission errors were set to $\pm 100\%$ for all regions (Section 3.4) and we tested the sensitivity of our posterior emissions to this value. **Figure 4** illustrates this by presenting posterior CH_2Cl_2 and C_2Cl_4 emissions for seven of the most important inversion regions under different prior error assumptions applied to each region simultaneously. Note, for this analysis a 0% error simply represents the prior emission. As errors are progressively increased each of the inversion regions are given a greater degree of freedom to reach a target. There are several features apparent in **Figure 4** that warrant attention. For CH_2Cl_2 , Temperate North America and Europe are examples of regions whose emission magnitudes are insensitive to the uncertainty assumed for the prior when it is above $\sim 50\%$. The Temperate and Tropical Asian regions were found to vary more with the assumed prior uncertainty, and the derived emissions are slightly anti-correlated. However, our Combined Asia region is insensitive to prior error when assumed to be equal or larger than $\pm 100\%$ (**Figure 4a**). Temperate Latin America is an example of a region that reaches its optimum emission value at a larger emissions error than $\pm 100\%$, and at further increased error drifts negatively. As previously noted, our posterior CH_2Cl_2 emissions from this region are negative, possibly reflecting a small inversion artefact due to the lack of data, but are also very small and thus of limited global importance: -0.96 (± 5.62) Gg yr⁻¹ in 2017. A similar sensitivity analysis to prior errors for the with ocean CH_2Cl_2 case was also performed (**Figure S3**).

For C_2Cl_4 , the posterior emissions are generally stable beyond $\pm 100\%$ prior error. Again, Temperate and Tropical Asia have a small tendency to drift towards each other, though likewise the Combined Asia region is insensitive to prior error, justifying our initial assumption, but only at errors beyond $\pm 200\%$ (**Figure 4b**).

4.6 Posterior versus Prior emissions performance

With prior and posterior CH_2Cl_2 and C_2Cl_4 emissions calculated, their performance can be evaluated by comparing modelled mixing ratios obtained with each to observations. We first focus on a single year (2016) and consider how well the posterior emissions reproduce background NOAA and AGAGE surface observations. Both the NOAA and AGAGE data used in these comparisons were assimilated by the inversion (i.e. to construct the posterior emissions). Comparisons to independent observational data are considered in Section 4.7. Modelled monthly mean CH_2Cl_2 (“no ocean” inversion) and C_2Cl_4 are compared to NOAA measurements in **Figures S4** and **S5**, respectively. For CH_2Cl_2 , **Figure S4** reveals generally very good agreement between the model (posterior emissions) and the observations. At several sites, particularly those at mid- and high latitudes in the Northern Hemisphere (NH), the prior and posterior emissions perform similarly. However, a clear improvement is obtained when using the posterior emissions in the tropics and in the Southern Hemisphere (SH). For C_2Cl_4 , posterior improvements at NOAA sites are more striking. **Figure S5** shows that our prior C_2Cl_4 emissions were too large, leading to a significant overestimation of observed mole fractions.

Similar comparisons but for AGAGE observations (converted to the NOAA calibration scale) are shown in **Figures S6** and **S7**. These comparisons are also for the year 2016, with the exception of the Gosan (GSN) site in South Korea (2015). For CH_2Cl_2 , the baseline measurements are better reproduced using our posterior emissions at most sites, except for ZEP, though as noted above the differences between prior and posterior results are relatively small in the NH. For C_2Cl_4 , again the posterior emissions lead to much better agreement between the model and observations. A notable feature for CH_2Cl_2 in **Figure S6**, apparent when using both the prior and posterior emissions, is the model overestimation of baseline CH_2Cl_2 observations at Gosan. This site is heavily influenced by several large nearby sources and the mismatch errors in the inversion are particularly large. Significantly improved agreement to the Gosan data is, however, obtained when the ‘raw’ measurements are used to construct monthly means (i.e. without filtering out pollution events). Such events are inheritably included in the model monthly means.

The comparisons discussed above focused on a single recent year. A more informative approach is to consider the performance of the posterior emissions over the entire study period. To quantify this performance, we calculate the mean absolute deviation (**Equation 7**) over the full study periods at each available NOAA site (14 for CH_2Cl_2 , 12 for C_2Cl_4) based on monthly means:

$$\text{mean absolute deviation} = \frac{\sum_{\text{months}} |\text{model} - \text{observation}|}{n_{\text{months}}} \quad \text{Equation 7.}$$

For CH_2Cl_2 , the posterior emissions provide much improved agreement to the observations at all sites, reducing the model/observation deviation to below ~5 ppt at most NH sites and below ~0.9 ppt at all SH sites (**Figure 5a**). This is not entirely unexpected given that these observations were included in the inversion itself. However, overall the reduction of the prior deviations by roughly 60% in the posterior indicates that the inversion procedure has been successful. C_2Cl_4 is equally successful, also with an average deviation reduction of roughly 80%, and 40% when the C_2Cl_4 + Cl sink is included (**Figure 5b**). Evident from the same figure, the magnitude of these improvements is not overly sensitive to inclusion of the +Cl sink, but the decreased reduction is due to the reduction in the prior deviations.

In addition to the above deviations, it is important that the time-dependent posterior emissions adequately capture trends. The four NOAA sites shown in **Figure 6** for CH_2Cl_2 are a selection from various geographical locations (**Table 1**): a high latitude NH site (ALT), a mid-latitude

NH site (LEF), a tropical site (KUM), and an SH site (CGO). The posterior CH_2Cl_2 model output is far better at matching with the observations over the 12-year period compared to the prior model output. This is especially true of the earlier parts of our study period given that our prior emissions (for the main industrialised regions) were based on bottom-up data from 2016. Annotated in **Figure 6** are the modelled (posterior) and observed CH_2Cl_2 trends over the 2006–2017 period, calculated using a simple least squares regression. The modelled and observed trends are 3.0 and 2.9 ppt yr⁻¹ at ALT, 2.8 and 3.0 ppt yr⁻¹ at LEF, 2.6 and 2.9 ppt yr⁻¹ at KUM, and 0.7 and 0.7 ppt yr⁻¹ at CGO, and thus are in excellent agreement. Despite the geographical range of the three NH sites, similar trends, roughly 3 ppt yr⁻¹, are found.

A similar analysis for C_2Cl_4 was performed at the same 4 sites, with again good agreement between the model (with posterior emissions) and the observations (**Figure 7**). The modelled and observed trends without the C_2Cl_4 + Cl sink reaction included are -0.14 and -0.13 ppt yr⁻¹ at ALT, -0.15 and -0.12 ppt yr⁻¹ at LEF, -0.07 and 0.08 yr⁻¹ at KUM, and -0.02 and -0.01 ppt yr⁻¹ at CGO. In addition, **Figure 7** includes the Cl sink of C_2Cl_4 . The trends are slightly improved in the posterior for three of the sites (except KUM), and the figure shows the stark contrast between the two prior model outputs. The addition of the Cl sink leads to a decreased lifetime of C_2Cl_4 [Hossaini et al., 2019], and therefore prior concentrations are decreased. The inversion compensates for this by increasing posterior emissions, as shown in **Figure 3**. Despite two very different prior positions, the two almost identical C_2Cl_4 posterior outputs (in **Figure 5b** and **Figure 7**) indicate how effective the inversion process can be.

Note, for CH_2Cl_2 the discussion above has focussed on the “no ocean” inversion. The posterior modelled CH_2Cl_2 mixing ratios from the with ocean inversion (not shown) are found to be almost identical, thus the performance of the two inversions is very similar. This implies that it cannot be concluded (or excluded) that a significant ocean CH_2Cl_2 source exists from this analysis.

4.7 Independent Observations

In the previous section we compared modelled CH_2Cl_2 and C_2Cl_4 mixing ratios, generated using our posterior emissions, to observations used in the inversion itself. Here, we examine independent observations, first considering aircraft measurements during the 2014 CAST, CONTRAST, and ATTREX missions over the tropical West Pacific (Section 3.2). Modelled and observed vertical profiles (surface to ~20 km) are displayed in **Figure 8**. Throughout the vertical extent of these profiles, there is (a) near-perfect agreement between modelled CH_2Cl_2 using the posterior emissions (“no ocean” inversion) compared to the observations, and (b) a significant improvement over the prior. The latter presumably reflects the larger Asian emissions in our posterior model occurring in the vicinity to the measurement campaigns. For C_2Cl_4 (CONTRAST and ATTREX only), **Figure 8b** shows results from the model both with and without the Cl sink. In both cases, the posterior emissions outperform the prior. The Cl sink case matches with the observations more effectively at higher altitudes, whereas both cases are similar towards the surface. On average, the model output overestimates C_2Cl_4 by 0.53 ppt for the no Cl sink and by 0.47 ppt for the Cl sink case. This overestimation could be caused by the large Combined Asia emissions, which heavily influence these observations.

The second test for our inversion is from the independent network of NOAA tall tower sites (USA-based, e.g. see **Figure 1**). At each of the 10 sites where CH_2Cl_2 observations are available, the posterior model provides a reasonable representation of the measurements in 2015 (**Figure 9**). Annotated on this figure are the mean absolute deviations at each site between the model (with prior and with posterior emissions) versus the observations, in that year. At most sites, the posterior model outperforms the prior, but generally only small improvements

in the CH_2Cl_2 average deviation are achieved. The correlations between model and observations (also annotated) also show a consistent improvement for the posterior. At certain sites, large standard deviations on the monthly mean observations coincide with poor model-measurement agreement, in some months. For example, the proximity of the MWO site to large urban areas may partly explain why the monthly mean observations are consistently larger than the model outputs, and for the other instances where large standard deviations occur, the model outputs lie at the lower range of the observations. For C_2Cl_4 , a similar analysis was performed and reveals a more varied picture (**Figure 10**). As prior emissions generally overestimate C_2Cl_4 this leads to large improvements in the posterior output at most sites. However, at some sites the modelled-observed C_2Cl_4 deviations are larger for the posterior compared to the prior (e.g. BAO and MWO). As for CH_2Cl_2 , this is largely due to the close proximity of substantial sources influencing observations that are likely not well captured by the model. However, at most sites we note that our posterior model output lies within the observed variability. We further note that as with all comparisons of relatively coarse global-scale models with point-based observations, sampling errors in the model can affect such comparisons.

For Europe, beyond the NOAA and AGAGE observational data used in the inversion, there are few long-term surface measurements of CH_2Cl_2 and C_2Cl_4 . However, a recent network addition is the establishment of a CH_2Cl_2 record at the Taunus Observatory (50.22°N , 8.44°E , at 825 m) in central Germany [Schuck et al., 2018]. Taunus reports CH_2Cl_2 measurements using the AGAGE SIO-14 scale (here converted to the NOAA scale). **Figure 11a** compares modelled and observed monthly mean CH_2Cl_2 at the Taunus site between 2014 and 2017. The agreement between the model (with posterior emissions) and observations is reasonable, with the shape of the seasonal cycle generally well captured. The model does overestimate CH_2Cl_2 at this particular site during some periods. Since sampling errors in the model could cause this overestimation, **Figure 11** also investigates model variability by including the standard deviation between the 8 neighbouring model grid cells, using **Equation 4**. At this particular site, variability introduced from neighbouring model grid cells is reasonably small and does not fully rationalise the small discrepancies between the model and observations, including apparent slight offsets in the seasonal cycle. However, we note that at other NH sites – including from the USA-based tall tower network – the CH_2Cl_2 seasonal cycle is very well captured (e.g. **Figures S4, S6 and 9**).

Also included in **Figure 11** are comparisons of modelled CH_2Cl_2 and C_2Cl_4 using our posterior emissions to baseline measurements obtained from the AGAGE-affiliated site in Hateruma, Japan (HAT, 24.1°N , 123.8°E , at 46.5 m). Hateruma is calibrated with the NIES-08 scale, and for CH_2Cl_2 can be converted to the AGAGE SIO-14 scale by a factor of 1.066 ± 0.008 . The conversion factor between the NIES-08 scale and AGAGE's NOAA-2003B scale for C_2Cl_4 is 0.994 ± 0.010 . Given that the number of monitoring stations in Asia is limited and that this is where the largest Cl-VSLs emissions are predicted to occur, these independent comparisons are particularly useful. For CH_2Cl_2 , model-observation agreement is generally good, though in the most recent years of our study period, the model underestimates observed CH_2Cl_2 mixing ratios, particularly in winter. This wintertime disparity could represent a combination of uncaptured seasonality in CH_2Cl_2 emissions and underestimated model CH_2Cl_2 lifetime, and is apparent even when considering the model sampling/mismatch issues noted above. For C_2Cl_4 , comparisons to the Hateruma data are shown for the model with and without the Cl sink used to construct the posterior emissions. Both cases lead to adequate model-measurement agreement, though including the Cl sink provides far better agreement in the most recent years.

5. Summary and Conclusions

Combining long-term surface observations and a chemical transport model, we have performed a global-scale synthesis inversion to (a) constrain regional/global emissions of CH_2Cl_2 and C_2Cl_4 , (b) investigate emission trends over the 2006 to 2017 period, and (c) produce a set of evaluated emission inventories for future global modelling studies. Our main findings are:

- For an inversion in which only industrial CH_2Cl_2 emissions are considered, we estimate that global CH_2Cl_2 emissions increased from $637 \pm 37 \text{ Gg yr}^{-1}$ in 2006 to $1171 \pm 45 \text{ Gg yr}^{-1}$ in 2017, with reasonably good agreement between our results and those reported in the recent WMO Ozone Assessment with a simplified model and similar data as input [Engel and Rigby et al., 2018]. This increase is largely attributed to an increase in Asian emissions, while relatively small European and North American emissions decrease over the same period. This geographical shift in the emission distribution is broadly consistent with studies that have highlighted the growing importance of major Asian economies as a CH_2Cl_2 source [e.g. Leedham Elvidge et al., 2015; Feng et al., 2018]. In 2017, we estimate Asian emissions accounted for 89% ($1045 \pm 40 \text{ Gg yr}^{-1}$) of total CH_2Cl_2 emissions, up from 68% ($431 \pm 32 \text{ Gg yr}^{-1}$) in 2006. CH_2Cl_2 emissions from Europe and North America combined represented 9% of the global total in 2017, down from 29% in 2006. Decreases in these regions may, in part, reflect recent concerns over the compound's toxicity in consumer products.
- For an inversion in which both oceanic and industrial CH_2Cl_2 sources are considered, we estimate global CH_2Cl_2 emissions of $1166 \pm 64 \text{ Gg yr}^{-1}$ in 2017; i.e. very similar to the no ocean case. However, including the ocean source reduces the estimate of 2017 Asian emissions from $1045 \pm 40 \text{ Gg yr}^{-1}$ to $886 \pm 53 \text{ Gg yr}^{-1}$ (a reduction of 15%). A large portion of this difference is explained by the inversion placing a significant emission of CH_2Cl_2 in the tropical Northern Ocean ($0\text{--}30^\circ\text{N}$ latitude). Averaged over our study period, oceanic CH_2Cl_2 emissions from this latitude band are $\sim 123 (\pm 45) \text{ Gg yr}^{-1}$, which is comparable to $88 (\pm 29) \text{ Gg yr}^{-1}$ for the same band estimated from a previous inversion study using primarily the same observational data as input but for an earlier time period (Xiao, 2008). The inclusion of an ocean source does not affect our overarching conclusions on a shift in global CH_2Cl_2 emissions, with an increasing contribution from Asia, and a declining contribution from Europe and North America since the mid-2000s. Additionally, comparisons of atmospheric measurements between this and the “no ocean” inversion lead to no evidence for (or against) an ocean CH_2Cl_2 source.
- Unlike CH_2Cl_2 , which has increased in the atmosphere since the early/mid 2000s, C_2Cl_4 has been in long-term decline. Our results indicate a decrease in global emissions from $141 \pm 14 \text{ Gg yr}^{-1}$ in 2007 to $106 \pm 12 \text{ Gg yr}^{-1}$ in 2017. These values were obtained from an inversion set up in which the $\text{C}_2\text{Cl}_4 + \text{Cl}$ sink reaction was not included and agree well with estimates produced for the recent WMO Ozone Assessment using a simplified model and similar input data [Engel and Rigby et al., 2018]. Inclusion of the $\text{C}_2\text{Cl}_4 + \text{Cl}$ reaction, shown to be an important, albeit uncertain, sink of C_2Cl_4 in recent modelling studies [Hossaini et al., 2019], increases the estimated global C_2Cl_4 emissions to $216 \pm 14 \text{ Gg yr}^{-1}$ in 2007 and $162 \pm 12 \text{ Gg yr}^{-1}$ in 2017; i.e. around 50% larger. Further work to constrain tropospheric Cl atom concentrations may help to constrain top-down emission estimates. Inclusion of the sink generally leads to slight improvements compared to the default inversion when comparing against atmospheric measurements.

- Using observational data not included in the inversion, the performance of the posterior CH_2Cl_2 and C_2Cl_4 emissions was evaluated. For both compounds, observed surface trends between the mid-2000s and 2017 are well reproduced: $\sim 3 \text{ ppt CH}_2\text{Cl}_2 \text{ yr}^{-1}$ and $\sim -0.1 \text{ ppt C}_2\text{Cl}_4 \text{ yr}^{-1}$ at NH sites. Independent measurements from the 2014 CAST/CONTRAST/ATTREX aircraft missions over the tropical West Pacific are also reproduced very well throughout the vertical extent of the troposphere for CH_2Cl_2 , and relatively less successfully for C_2Cl_4 . Similarly, the posterior emissions show improvement over the prior at numerous USA-based NOAA tall tower sites in 2015. Comparisons for other surface sites were performed, including Taunus Observatory (Germany) and Hateruma (Japan), and reveal generally good agreement. Our emissions are thus suitable for inclusion in global atmospheric modelling studies.

In conclusion, emissions of CH_2Cl_2 – a known ozone-depleting substance – have increased significantly since the mid-2000s. Given that Asian emissions lead to a relatively large CH_2Cl_2 ozone depletion potential [Claxton et al., 2019], its regional and global abundance should continue to be monitored. As emissions from the Asian continent are by far the largest, a denser set of measurements, from the surface to the tropopause, would be beneficial to distinguish emissions from different subregions and ultimately constrain the troposphere-to-stratosphere input of chlorine from VSLS. A consideration of how emissions are likely to change in coming decades would also help constrain the influence of CH_2Cl_2 on the timescale of stratospheric ozone recovery. Future work should also focus on elucidating the mechanism by which CH_2Cl_2 is recycled through the ocean and quantifying the magnitude and distribution of biogenic sources.

Acknowledgements

This work was supported by RH's NERC Independent Research Fellowship (NE/N014375/1), the NERC ISHOC project (NE/R004927/1) and the NERC SISLAC project (NE/R001782/1). MPC is supported by a Wolfson Merit Award. We thank Dr Wuhu Feng for his work developing the TOMCAT/SLIMCAT model. We thank Dr Prabir Patra and Dr Bin Xiang for providing the HCFC-22 emission distribution. LJC thanks NERC for funding the CAST and ship observations (NE/J00619X/1, NE/K004980/1 and NE/I028769/1). Data from the NOAA monitoring network are available from: <https://www.esrl.noaa.gov/gmd/>. We thank C. Siso for technical assistance in making the NOAA measurements, and Dr B. Miller and Dr A. Andrews for assistance in providing results from NOAA's tall tower network. Gosan measurements were supported by Basic Science Research Program through the National Research Foundation of Korea (NRF) funded by the Ministry of Education (No. 2017R1D1A1B03034034). The operation of the AGAGE station at Ragged Point, Barbados, is supported by the National Aeronautics and Space Administration (NASA, USA; grant NNX16AC98G to MIT, sub-award 5710002970 to the University of Bristol) with additional support from the National Oceanic and Atmospheric Administration (NOAA, USA; contract RA133R15CN0008 to the University of Bristol). Observations at Hateruma were partly supported by the Ministry of the Environment of Japan. Data from the AGAGE monitoring network are available from <https://agage.mit.edu/data/> and are supported by the NASA Upper Atmospheric Research Program in the US with grants NNX16AC96G and NNX16AC97G to SIO, and grant NNX16AC98G to MIT. ATTREX and CONTRAST measurements were supported by National Science Foundation grant #AGS1261689 and NASA grant # NNX13AH20G. The model data can be accessed via the Lancaster University data repository at DOI: 10.17635/lancaster/researchdata/353. The Supporting Information to this article consists of 7 figures and 3 tables.

References

- Andrews, S. J., Hackenberg, S. C., & Carpenter, L. J. (2015). Technical Note: A fully automated purge and trap GC-MS system for quantification of volatile organic compound (VOC) fluxes between the ocean and atmosphere, *Ocean Science*, **11**, 313-321, <https://doi.org/10.5194/os-11-313-2015>.
- Andrews, S. J., Carpenter, L., Apel, E., Atlas, E., Donets, V., Hopkins, J. R., et al. (2016). A comparison of very short lived halocarbon (VSLS) and DMS aircraft measurements in the tropical west Pacific from CAST, ATTREX and CONTRAST, *Atmospheric Measurement Techniques*, **9**, 5213-5225. <https://doi.org/10.5194/amt-9-5213-2016>.
- Ashfold, M. J., Pyle, J. A., Robinson, A. D., Meneguz, E., Nadzir, M. S. M., Phang, S. M., et al. (2015). Rapid transport of East Asian pollution to the deep tropics. *Atmospheric Chemistry and Physics*, **15**(6), 3565–3573. doi:10.5194/acp-15-3565-2015.
- Baker, D. F., Law, R. M., Gurney, K., Rayner, P., Peylin, P., Denning, A. S., et al. (2006). TransCom 3 inversion intercomparison: Impact of transport model errors on the interannual variability of regional CO₂ fluxes, 1988-2003, *Global Biogeochemical Cycles*, **20**(1), [GB1002]. <https://doi.org/10.1029/2004GB002439>.
- Bousquet, P., Yver, C., Pison, I., Li, Y. S., Fortems, A., Hauglustaine, D., et al. (2011). A three-dimensional synthesis inversion of the molecular hydrogen cycle: Sources and sinks budget and implications for the soil uptake, *Journal of Geophysical Research*, **116**, D01302, doi:10.1029/2010JD014599.
- Burkholder, J. B., Sander, S. P., Abbatt, J., Barker, J. R., Huie, R. E., Kolb, C. E., et al. (2015). Chemical kinetics and photochemical data for use in atmospheric studies, Evaluation number 18, *JPL Publication 15-10*, Jet Propulsion Laboratory, Pasadena. <http://jpldataeval.jpl.nasa.gov/>
- Carpenter, L. J., Reiman, S., Burkholder, J. B., Clerbaux, C., Hall, B. D., Hossaini, R., et al. (2014). Ozone-depleting substances (ODSs) and other gases of interest to the Montreal Protocol. In *Scientific assessment of ozone depletion: 2014, global ozone research and monitoring project - Report No. 55*, World Meteorological Organization, Geneva, Switzerland.
- Chen, Y.-H., & Prinn, R. G. (2006). Estimation of atmospheric methane emissions between 1996 and 2001 using a three-dimensional global chemical transport model, *Journal of Geophysical Research*, **111**, D10307, doi:10.1029/2005JD006058.
- Chipperfield, M. P. (2006). New version of the TOMCAT/SLIMCAT off-line chemical transport model: Intercomparison of stratospheric tracer experiments, *Quarterly Journal of the Royal Meteorological Society*, **132**(617), 1179–1203. <http://doi.org/10.1256/qj.05.51>.
- Claxton, T., Hossaini, R., Wild, O., Chipperfield, M. P., and Wilson, C. (2019). On the regional and seasonal ozone depletion potential of chlorinated very short-lived substances, *Geophysical Research Letters*, **46**(10), 5489-5498. doi:10.1029/2018GL081455.
- Cunnold, D. M., Prinn, R. G., Rasmussen, R. A., Simmonds, P. G., Alyea, F. N., Cardelino, C. A., et al. (1983). The atmospheric lifetime experiment: 3. Lifetime methodology and application to three years of CFCl₃ data, *Journal of Geophysical Research: Oceans*, **88**, 8379-8400, doi.org/10.1029/JC088iC13p08379.
- Dee, D., Uppala, S., Simmons, A., Berrisford, P., Poli, P., Kobayashi, S., et al. (2011). The ERA-Interim reanalysis: Configuration and performance of the data assimilation system,

Quarterly Journal of the Royal Meteorological Society, **137**(656), 553–597.
<https://doi.org/10.1002/qj.828>.

Engel, A., Rigby, M., Burkholder, J. B., Fernandez, R. P., Froidevaux, L., Hall, B. D., et al. (2018). Update on ozone-depleting substances (ODSs) and other gases of interest to the Montreal Protocol. In *Scientific assessment of ozone depletion: 2018, global ozone research and monitoring project-Report No. 58*, World Meteorological Organization, Geneva, Switzerland.

Fang, X., Park, S., Saito, T., Tunnicliffe, R., Ganesan, A. L., Rigby, M., et al. (2019). Rapid increase in ozone-depleting chloroform emissions from China, *Nature Geoscience*, **12**, 89–93, doi.org/10.1038/s41561-018-0278-2.

Feng, Y., Bie, P., Wang, Z., Wang, L., & Zhang, J. (2018). Bottom-up anthropogenic dichloromethane emission estimates from China for the period 2005–2016 and predictions of future emissions, *Atmospheric Environment*, **186**, 241–247.
<https://doi.org/10.1016/j.atmosenv.2018.05.039>.

Fernandez R. P., Salawitch R. J., Kinnison D. E., Lamarque J. -F., and Saiz-Lopez A. (2014). Bromine partitioning in the tropical tropopause layer: Implications for stratospheric injection, *Atmospheric Chemistry and Physics*, **14**, 13,391–13,410, doi: 10.5194/acp-14-13391-2014.

Hackenberg, S. C., Andrews, S. J., Airs, R., Arnold, S. R., Bouman, H. A., Brewin, R. J. W., et al. (2017). Potential controls of isoprene in the surface ocean, *Global Biogeochemical Cycles*, **31**, 644–662, doi:10.1002/2016GB005531.

Harris, N. R. P., Carpenter, L. J., Lee, J. D., Vaughan, G., Filus, M. T., Jones, R. L., et al. (2017). Co-ordinated Airborne Studies in the Tropics (CAST), *B. American Meteorological Society*, **Issue**, doi:10.1175/BAMS-D-1400290.1.

Hossaini, R. (2020): TOMCAT Model Data for Chlorinated VSLs 2019. Lancaster University. [10.17635/lancaster/researchdata/353](https://doi.org/10.17635/lancaster/researchdata/353).

Hossaini, R., Chipperfield, M. P., Monge-Sanz, B. M., Richards, N. A. D., Atlas, E., & Blake, D. R. (2010). Bromoform and dibromomethane in the tropics: A 3-D model study of chemistry and transport, *Atmospheric Chemistry and Physics*, **10**, 719–735, doi:10.5194/acp-10-719-2010.

Hossaini, R., Chipperfield, M. P., Saiz-Lopez, A., Fernandez, R., Monks, S., Feng, W., Brauer, P., & von Glasow, R. (2016). A global model of tropospheric chlorine chemistry: Organic versus inorganic sources and impact on methane oxidation, *Journal of Geophysical Research*, **121**, 14271–14297, doi:10.1002/2016JD025756.

Hossaini, R., Chipperfield, M. P., Montzka, S. A., Leeson, A. A., Dhomse, S. S., & Pyle, J. A. (2017). The increasing threat to stratospheric ozone from dichloromethane, *Nature Communications*, **8**, 1–9. <https://doi.org/10.1038/ncomms15962>.

Hossaini, R., Atlas, E., Dhomse, S. S., Chipperfield, M. P., Bernath, P. F., Fernando, A. M., et al. (2019). Recent trends in stratospheric chlorine from very short-lived substances, *Journal of Geophysical Research: Atmospheres*. <https://doi.org/10.1029/2018JD029400>

Huijnen, V., Williams, J., van Weele, M., van Noije, T., Krol, M., Dentener, F., et al. (2010). The global chemistry transport model TM5: Description and evaluation of the tropospheric chemistry version 3.0, *Geoscience Model Development*, **3**, 445–473.

Johnson, M. T. (2010). A numerical scheme to calculate temperature and salinity dependent air-water transfer velocities for any gas, *Ocean Science*, **6**(4), 913–932, doi:10.5194/os-6-913-2010.

Jones, C. E., & Carpenter, L. J. (2005). Solar photolysis of CH₂I₂, CH₂ICl, and CH₂IBr in water, saltwater, and seawater, *Environmental Science and Technology*, **39**, 6130-6137, doi:10.1021/es050563g.

Keene, W. C., Khalil, M. A. K., Erickson III, D. J., McCulloch, A., Graedel, T. E., Lobert, J. M., et al. (1999). Composite global emissions of reactive chlorine from anthropogenic and natural sources: Reactive chlorine emissions inventory, *Journal of Geophysical Research*, **104**, 8429–8440. <https://doi.org/10.1029/1998JD100084>.

Khalil, M. A. K., Moore, R. M., Harper, D. B., Lobert, J. M., Erickson, D. J., Koropalov, V., Sturges, W. T., & Keene W. C., (1999). Natural emissions of chlorine-containing gases: Reactive Chlorine Emissions Inventory, *Journal of Geophysical Research*, **104**(D7), 8333–8346, doi:10.1029/1998JD100079.

Khalil, M. A. K., & Rasmussen, R. A. (1999). Atmospheric Chloroform, *Atmospheric Environment*, **33**, 1151-1158, doi.org/10.1016/S1352-2310(98)00233-7

Kolusu, S., Schlünzen, H., Grawe, D., & Seifert, R. (2016). Chloromethane and dichloromethane in the tropical Atlantic Ocean, *Atmospheric Environment*, **150**, 417-424, doi: 10.1016/j.atmosenv.2016.11.037.

Kolusu, S. R., Schlünzen, K. H., Grawe, D., & Seifert, R. (2018). Determination of chloromethane and dichloromethane in a tropical terrestrial mangrove forest in Brazil by measurements and modelling, *Atmospheric Environment*, **173**, 185-197, doi.org/10.1016/j.atmosenv.2017.10.057.

Laube, J. C., Engel, A., Bönisch, H., Möbius, T., Worton, D. R., Sturges, W. T., Grunow, K., & Schmidt, U. (2008). Contribution of very short-lived organic substances to stratospheric chlorine and bromine in the tropics—A case study. *Atmospheric Chemistry and Physics*, **8**(23), 7325– 7334, doi.org/10.5194/acp-8-7325-2008.

Law, R. M., Peters, W., Rodenbeck, C., Aulagnier, C., Baker, I., Bergmann, D. J., Bousquet, P., & Brandt, J. (2008). TransCom model simulations of hourly atmospheric CO₂: Experimental overview and diurnal cycle results for 2002, *Global Biogeochemical Cycles*, **22**, GB3009, doi.

Lawson, S. J., Keywood, M. D., Galbally, I. E., Gras, J. L., Cainey, J. M., Cope, M. E., et al. (2015). Biomass burning emissions of trace gases and particles in marine air at Cape Grim, Tasmania, *Atmospheric Chemistry and Physics*, **15**, 13393-13411, <https://doi.org/10.5194/acp-15-13393-2015>.

Leedham Elvidge, E. C., Oram, D. E., Laube, J. C., Baker, A. K., Montzka, S. A., Humphrey, S., O'Sullivan, D. A., & Brenninkmeijer, C. A. M. (2015). Increasing concentrations of dichloromethane, CH₂Cl₂, inferred from CARIBIC air samples collected 1998-2012, *Atmospheric Chemistry and Physics*, **15**, 1939-1958. <https://doi.org/10.5194/acp-15-1939-2015>.

Lobert, J., Keene, W. C., Logan, J., & Yevich, R. (1999) Global chlorine emissions from biomass burning – Reactive Chlorine Emissions Inventory, *Journal of Geophysical Research*, **104**, 8373-8390, doi: 10.1029/1998JD100077.

- McCulloch, A., Aucott, M. L., Graedel, T. E., Kleiman, G., Midgley, M., & Li, Y-F. (1999). Industrial emissions of trichloroethene, tetrachloroethene, and dichloromethane: reactive chlorine emissions inventory, *Journal of Geophysical Research*, **104**, 8417-8427. doi:10.1029/1999JD900011.
- McCulloch, A., & Midgley, P. M. (1996). The production and global distribution of emissions of trichloroethene, tetrachloroethene and dichloromethane over the period 1988-1992, *Atmospheric Environment*, **30**, 601-608, doi:10.1016/1352-2310(09)50032-5.
- McNorton, J., Wilson, C., Gloor, M., Parker, R. J., Boesch, H., Feng, W., Hossaini, R., and Chipperfield, M. P. (2018). Attribution of recent increases in atmospheric methane through 3-D inverse modelling, *Atmospheric Chemistry and Physics*, **18**, 18149–18168, <https://doi.org/10.5194/acp-18-18149-2018>.
- Monks, S., Arnold, S. R., Hollaway, M., Pope, R., Wilson, C., Feng, W., et al. (2016) The TOMCAT global chemistry transport model: Description of chemical mechanism and model evaluation, *Geoscientific Model Development Discussions*, 1-51, doi: 10.5194/gmd-2016-212.
- Montzka, S. A., Dutton, G. S., Yu, P., Ray, E., Portmann, R. W., Daniel, J. S., et al. (2018). An unexpected and persistent increase in global emissions of ozone-depleting CFC-11, *Nature*, **557**, 413-417, doi.org/10.1038/s41586-018-0106-2.
- Montzka, S. A., Reimann, S., Engel, A., Kruger, K., O'Doherty, S., Sturges, W. T., et al., (2011). Ozone-depleting substances (ODSs) and related chemicals. In *Scientific assessment of ozone depletion: 2010, global ozone research and monitoring project-Report No. 52*, World Meteorological Organization, Geneva, Switzerland.
- Moore, R. M. (2004), Dichloromethane in North Atlantic waters, *Journal of Geophysical Research*, **109**, C09004, doi:10.1029/2004JC002397.
- Mühle, J., Lueker, T. J., Su, Y., Miller, B. R., Prather, K. A., & Weiss, R. F. (2007). Trace gas and particulate emissions from the 2003 southern California wildfires, *Journal of Geophysical Research*, **112**, D03307, doi:10.1029/2006JD007350.
- Mühle, J., Trudinger, C. M., Western, L.M., Rigby, M., Vollmer, M. K., Park, S. Manning, A. J., et al. (2019). Perfluorocyclobutane (PFC-318, c-C₄F₈) in the global atmosphere, *Atmospheric Chemistry and Physics*, **19**(15), 10335-10359, 10.5194/acp-19-10335-2019.
- Navarro, M. A., Atlas, E. L., Saiz-Lopez, A., Rodriguez-Lloveras, X., Kinnison, D. E., Lamarque, J., et al. (2015). Airborne measurements of organic bromine compounds in the Pacific tropical tropopause layer. *Proceedings of the National Academy of Sciences of the United States of America*, **112**(45), 13,789–13,793. <https://doi.org/10.1073/pnas.1511463112>.
- Ooki, A., & Yokouchi, Y. (2011). Dichloromethane in the Indian Ocean: Evidence for in-situ production in seawater, *Marine Chemistry*, **124**, 1-4, 119-124, doi: 10.1016/j.marchem.2011.01.001.
- Oram, D. E., Ashfold, M. J., Laube, J. C., Gooch, L. J., Humphrey, S., Sturges, W. T., et al. (2017). A growing threat to the ozone layer from short-lived anthropogenic chlorocarbons, *Atmospheric Chemistry and Physics*, **17**(19), 11,929–11,941. <https://doi.org/10.5194/acp-17-11929-2017>.
- Pan, L. L., Atlas, E. L., Salawitch, R. J., Honomichl, S. B., Bresch, J. F., Randel, W. J., Apel, E. C., & Hornbrook, R. S., (2017). The Convective Transport of Active Species in the Tropics

(CONTRAST) experiment, *Bulletin of the American Meteorological Society*, **98**, 106–128, <https://doi.org/10.1175/BAMS-D-14-00272.1>.

Patra, P. K., Houweling, S., Krol, M., Bousquet, P., Belikov, D., Bergmann, D., et al. (2011). TransCom model simulations of CH₄ and related species: linking transport, surface flux and chemical loss with CH₄ variability in the troposphere and lower stratosphere, *Atmospheric Chemistry and Physics*, **11**, 12813–12837, <https://doi.org/10.5194/acp-11-12813-2011>.

Pétron, G., Granier, C., Khattatov, B., Lamarque, J. F., Yudin, V., and someone, et al. (2002). Inverse modelling of carbon monoxide surface emissions using Climate Monitoring and Diagnostics Laboratory network observations, *Journal of Geophysical Research*, **107**(D24), 4761, <https://doi.org/10.1029/2001JD001305>.

Prinn, R. G., Huang, J., Weiss, R. F., Cunnold, D. M., Fraser, P. J., Simmonds, P. G., et al. (2005). Evidence for variability of atmospheric hydroxyl radicals over the past quarter century, *Geophysical Research Letters*, **32**, 10.1029/2004GL022228. Prinn, R. G., Weiss, R. F., Arduini, J., Arnold, T., DeWitt, H. L., Fraser, P. J., et al. (2018). History of chemically and radiatively important atmospheric gases from the Advanced Global Atmospheric Gases Experiment (AGAGE), *Earth System Science Data*, **10**, 985–1018, doi: 10.5194/essd-10-985-2018, 2018.

Quack, B., & Wallace, D. W. R. (2003). Air-sea flux of bromoform: Controls, rates, and implications. *Global Biogeochemical Cycles*, **17**(1), 1023, doi.org/10.1029/2002GB001890.

Rigby, M., Prinn, R. G., O'Doherty, S., Montzka, S. A., McCulloch, A., Harth, C. M., et al. (2013). Re-evaluation of the lifetimes of the major CFCs and CH₃CCl₃ using atmospheric trends, *Atmospheric Chemistry and Physics*, **13**, 2691–2702, doi.org/10.5194/acp-13-2691-2013.

Schuck, T. J., Lefrancois, F., Gallmann, F., Wang, D., Jesswein, M., Hoker, J., Bonisch, H., & Engel, A. (2018). Halocarbons at Taunus Observatory, *Atmospheric Chemistry and Physics*, **18**, 16553–16569, doi.org/10.5194/acp-18-16553-2018.

Simmonds, P. G., Manning, A. J., Cunnold, D. M., McCulloch, A., O'Doherty, S., Derwent, R. G., et al., (2006). Global trends, seasonal cycles, and European emissions of dichloromethane, trichloroethene, and tetrachloroethene from the AGAGE observations at Mace Head, Ireland, and Cape Grim, Tasmania, *Journal of Geophysical Research*, **111**, D18304, doi:10.1029/2006JD007082.

Simpson, I. J., Meinardi, S., Blake, N. J., Rowland, F. S., & Blake, D. R. (2004). Long-term decrease in the global atmospheric burden of tetrachloroethene (C₂Cl₄), *Geophysical Research Letters*, **31**, L08108, doi:10.1029/2003GL019351.

Simpson, I. J., Akagi, S. K., Barletta, B., Blake, N. J., Choi, Y., Diskin, G. S., et al., (2011). Boreal forest fire emissions in fresh Canadian smoke plumes: C₁–C₁₀volatile organic compounds (VOCs), CO₂, CO, NO₂, NO, HCN and CH₃CN, *Atmospheric Chemistry and Physics*, **11**, 6445–6463, <https://doi.org/10.5194/acp-11-6445-2011>.

Spivakovsky, C. M., Logan, J. A., Montzka, S. A., Balkanski, Y. J., Foreman-Fowler, M., Jones, D. B. A., et al. (2000). Three-dimensional climatological distribution of tropospheric OH: Update and evaluation, *Journal of Geophysical Research*, **105**, 8931–8980, doi:10.1029/1999JD901006.

Sturges W., Oram D., Carpenter L., Penkett S., & Engel A. (2000). Bromoform as a source of stratospheric bromine, *Geophysical Research Letters*, **27**(14), 2081–2084, doi:10.1029/2000GL011444.

Tarantola, A., & Valette, B. (1982). Generalized nonlinear inverse problems solved using the least squares criterion, *Reviews of Geophysics*, **20**, 219-232, doi:10.1029/RG020i002p00219.

Trudinger, C. M., Etheridge, D. M., Sturrock, G. A., Fraser, P. J., Krummel, P. B., & McCulloch, A. (2004). Atmospheric histories of halocarbons from analysis of Antarctic firn air: Methyl bromide, methyl chloride, chloroform and dichloromethane, *Journal of Geophysical Research*, **109**, doi:10.1029/2004JD004932.

Tsai, W. T., (2017). Fate of Chloromethanes in the Atmospheric Environment: Implications for Human Health, Ozone Formation and Depletion, and Global Warming Impacts, *Toxics*, **5**(4), 23, 10.3390/toxics5040023.

Turner, A. J., Fung, I., Naik, V., Horowitz, L. W., & Cohen, R. C. (2018). Modulation of hydroxyl variability by ENSO in the absence of external forcing, *Proceedings of the National Academy of Sciences*, **115**(36), 8931-8936, 10.1073/pnas.1807532115.

Wales, P. A., Salawitch, R. J., Nicely, J. M., Anderson, D. C., Canty, T. P., Baidar, S., et al. (2018). Stratospheric injection of brominated very short-lived substances: Aircraft observations in the Western Pacific and representation in global models. *Journal of Geophysical Research: Atmospheres*, **123**, 5690–5719, doi.org/10.1029/2017JD027978.

Wang, J. S., Kawa, S. R., Collatz, G. J., Sasakawa, M., Gatti, L. V., Machida, T., et al. (2018). A global synthesis inversion analysis of recent variable in CO₂ fluxes using GOSAT and in situ observations, *Atmospheric Chemistry and Physics*, **18**, 11097-11124, doi:10.5194/acp-18-11097-2018.

Xiang, B., Patra, P. K., Montzka, S. A., Miller, S. M., Elkins, J. W., Moore, F. L., et al. (2014). Global emissions of refrigerants HCFC-22 and HFC-134a: Unforeseen seasonal contributions, *Proceeding of the National Academy of Sciences of the United States of America*, **111**, 17379-17384, doi.org/10.1073/pnas.1417372111.

Xiao, X. (2008). *Optimal Estimation of the Surface Fluxes of Chloromethanes Using a 3-D Global Atmospheric Chemical Transport Model* (Doctoral dissertation). (https://globalchange.mit.edu/sites/default/files/Xiao_PhD_08.pdf). Cambridge, Massachusetts, USA: Massachusetts Institute of Technology.

Ziska, F., Quack, B., Abrahamsson, K., Archer, S. D., Atlas, E., Bell, T., et al. (2013). Global sea-to-air flux climatology for bromoform, dibromomethane and methyl iodide. *Atmospheric Chemistry and Physics*, **13**(17), 8915–8934, doi.org/10.5194/acp-13-8915-2013.

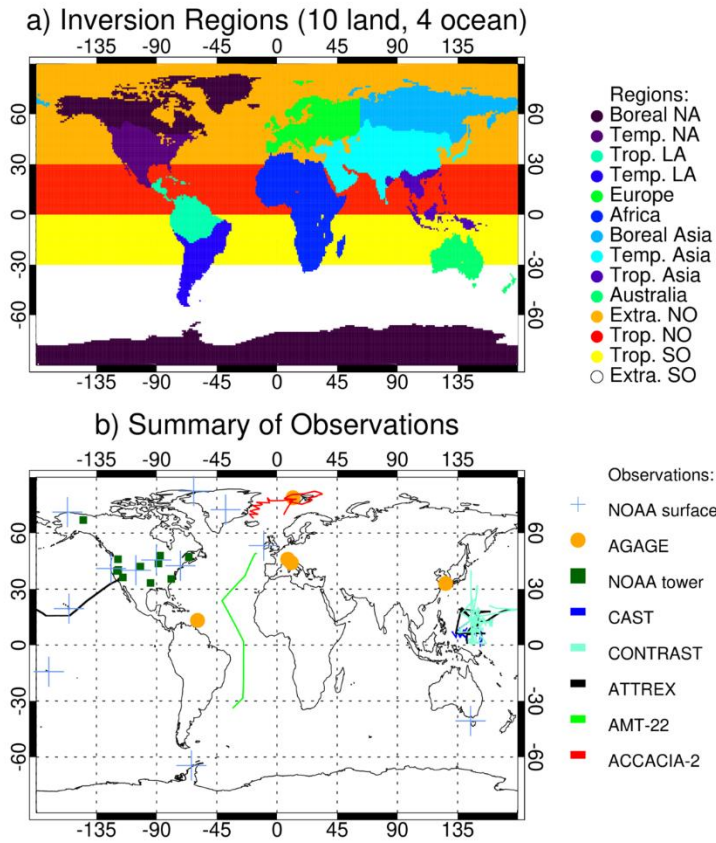


Figure 1. (a) Map showing the 14 regions (10 land, 4 ocean) used in the inversion. NA = North America, LA = Latin America, NO = Northern Ocean, SO = Southern Ocean, Extra. = Extratropical, Trop. = Tropical, Temp. = Temperate. (b) Summary of the various observations used in this study: NOAA surface sites (blue plusses); AGAGE surface sites (orange circles); NOAA tall tower sites (green squares). Flight campaigns: CAST (purple); ATTREX (black); CONTRAST (light blue). Ocean campaigns: AMT-22 (green); ACCACIA-22 (red).

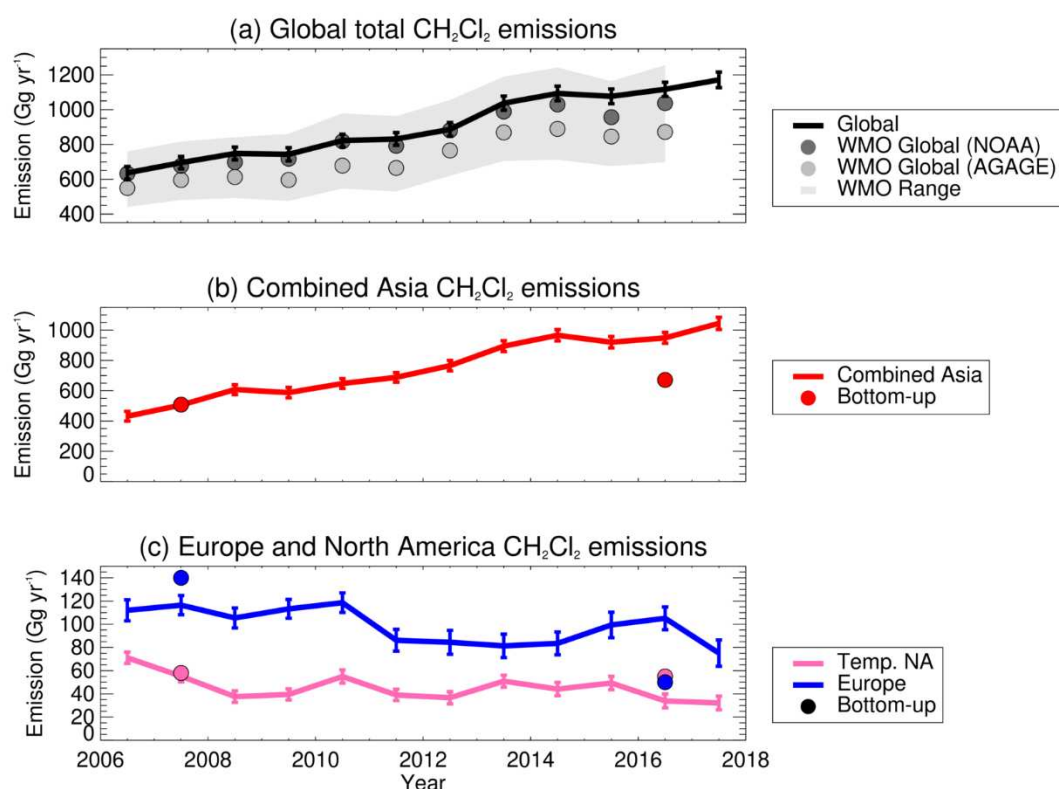


Figure 2. Timeseries of posterior CH_2Cl_2 emissions (Gg yr⁻¹) over the 12-year (2006-2017) study period. **(a)** Global total emissions from the inversion (black line, this work) alongside estimates from a 12-box model (circles) forced by NOAA (dark grey) and AGAGE (light grey) observations, as reported in Engel and Rigby et al. [2018]. The full 12-box model uncertainty range is represented by pale grey shading. **(b)** Asian emissions from the inversion showing Combined Asia (Temperate + Tropical), alongside bottom-up estimates from NSA (circles). **(c)** European and North American emissions, alongside bottom-up estimates from NSA (circles). See Section 3.4 for a description of the bottom-up data. Note, the CH_2Cl_2 results shown here are for the no oceanic emission scenario. Error bars represent uncertainty ranges included in Table 3.

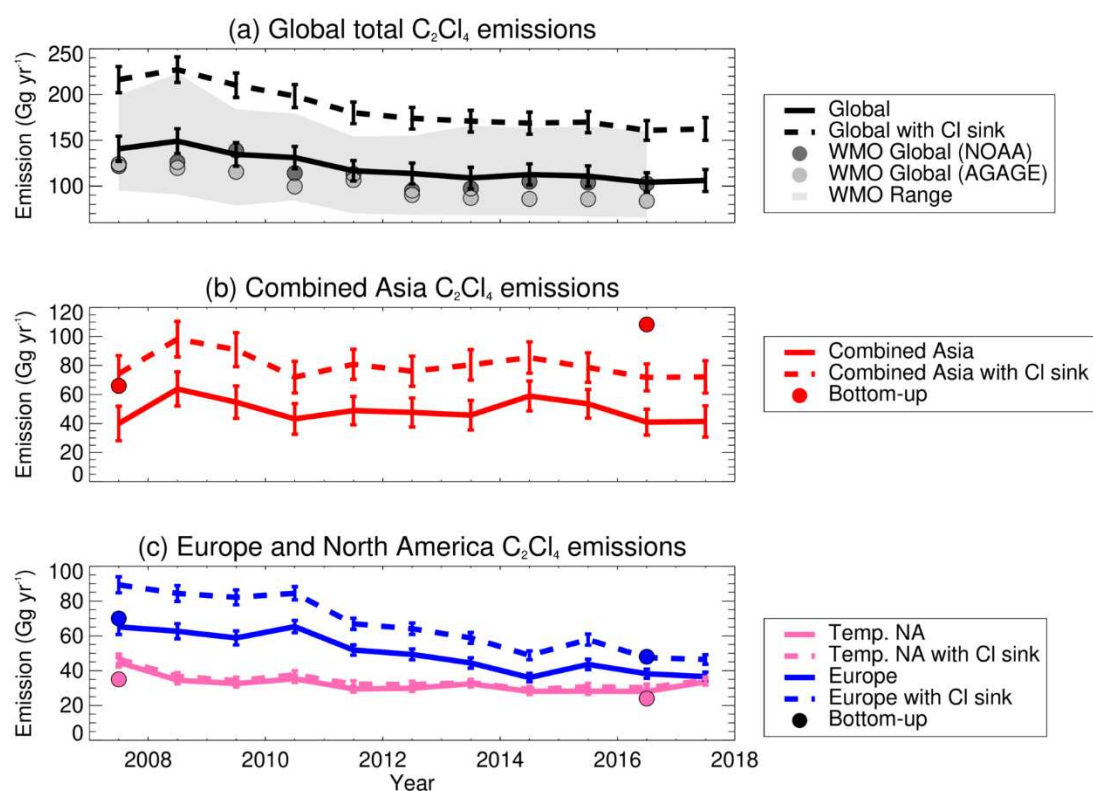


Figure 3. As Figure 2 but for C_2Cl_4 . Results are shown for simulations with (dashed line) and without (solid line) the $C_2Cl_4 + Cl$ sink reaction.

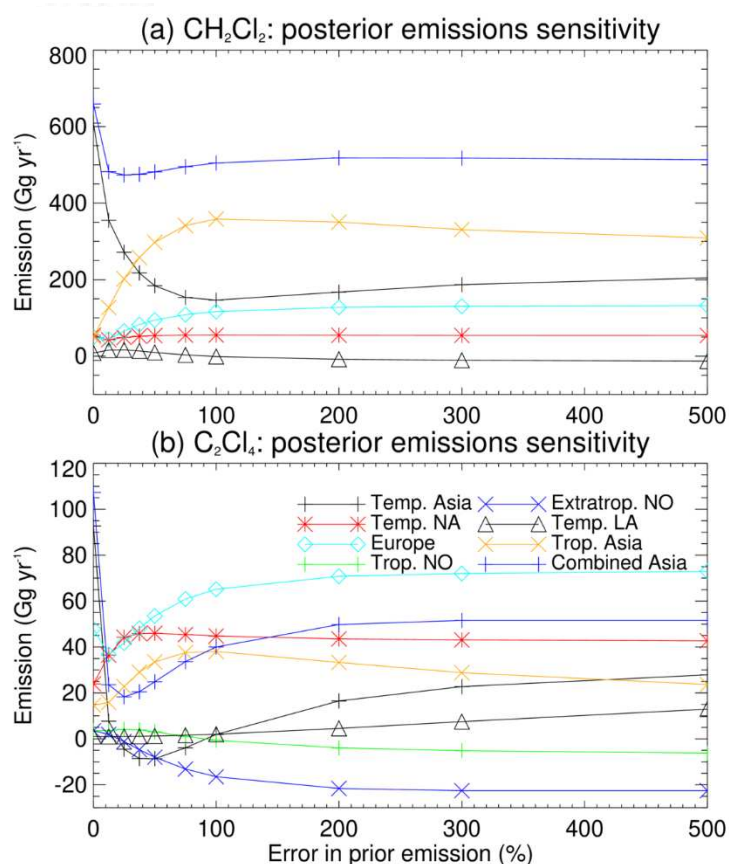


Figure 4. Summary of results testing the sensitivity of posterior emissions to the assumed error in the prior emissions for (a) CH_2Cl_2 and (b) C_2Cl_4 . Results are shown indicatively for the year 2007 and for 7 different regions (5 for CH_2Cl_2), including a Combined Asian result. Note, a 0% prior emission error equates to the prior emissions. For CH_2Cl_2 , results are shown for the no ocean inversion scenario.

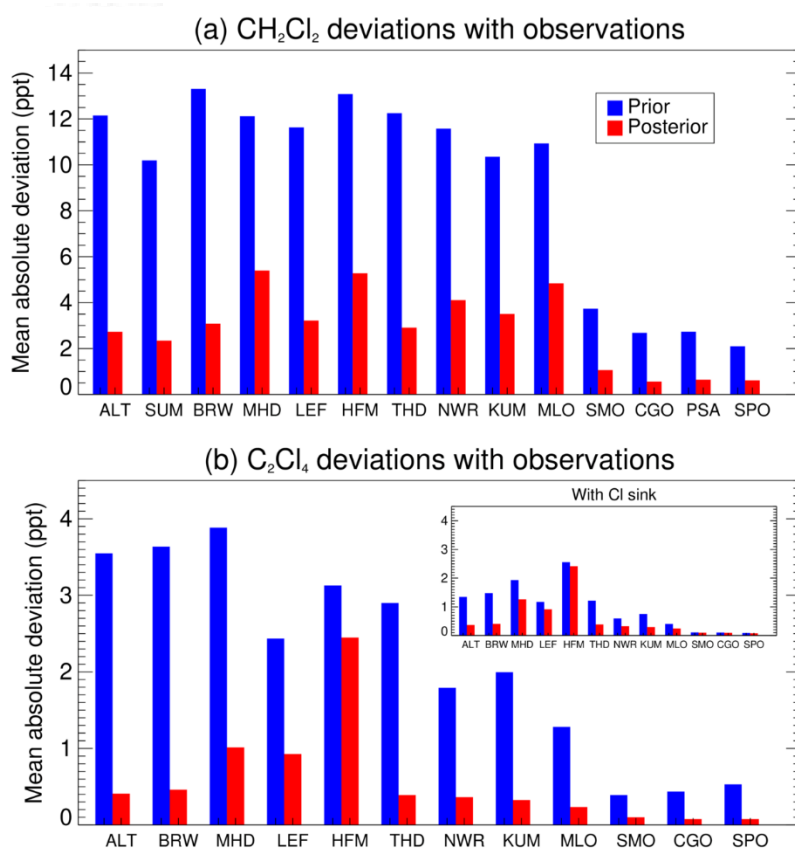


Figure 5. Mean absolute deviation (ppt) between modelled and observed (a) CH₂Cl₂ and (b) C₂Cl₄, at NOAA sites. The deviations are averages calculated from monthly mean data over the study periods (2006-2017 for CH₂Cl₂, 2007-2017 for C₂Cl₄) and are shown for model output generated using the prior emissions and the posterior emissions. The C₂Cl₄ + Cl sink comparisons are inset in (b). For CH₂Cl₂, results are generated using the posterior emissions from the no ocean inversion scenario.

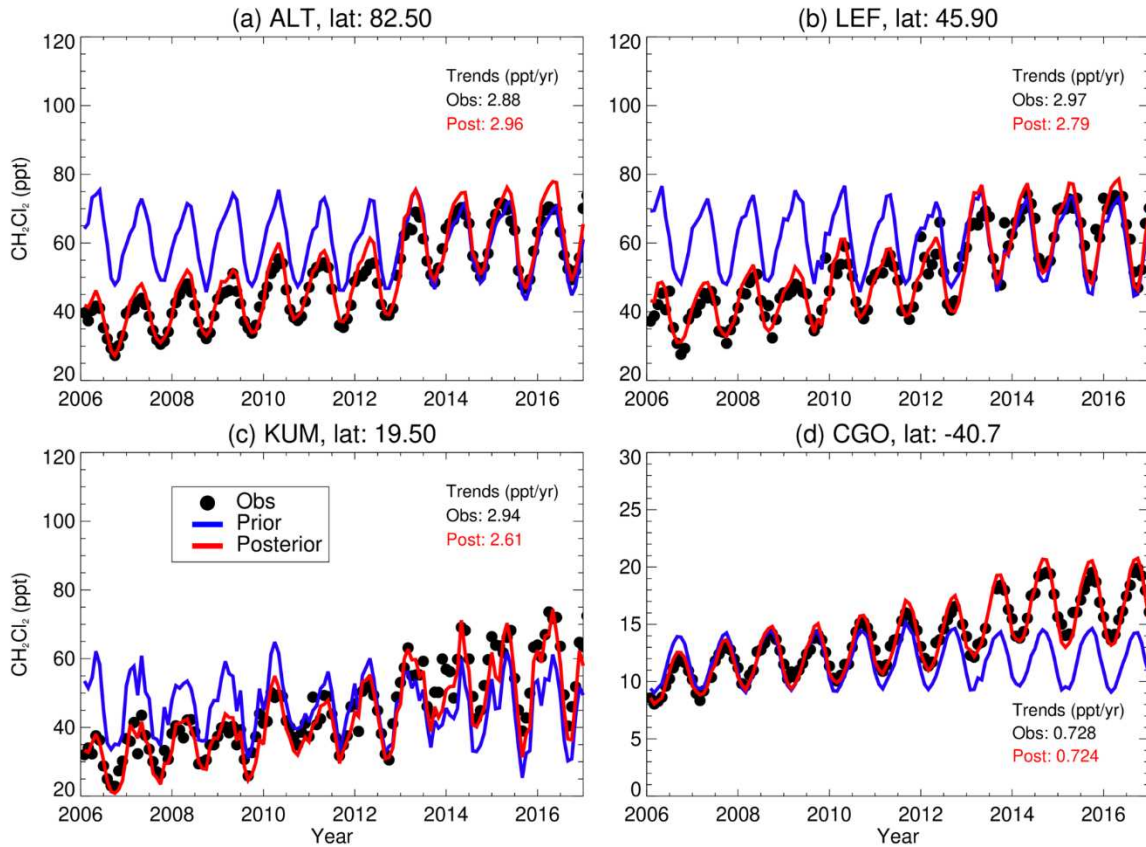


Figure 6. Comparison of modelled monthly mean CH_2Cl_2 mixing ratio (ppt) versus NOAA observations (2006-2017) at stations (a) ALT, (b) KUM, (c) LEF and (d) CGO. Each panel contains model output based on the prior (blue) and the posterior (red) emissions, with annual trends (ppt yr^{-1}) in the model (posterior) and observations annotated. For CH_2Cl_2 , results are generated using the posterior emissions from the no ocean inversion scenario.

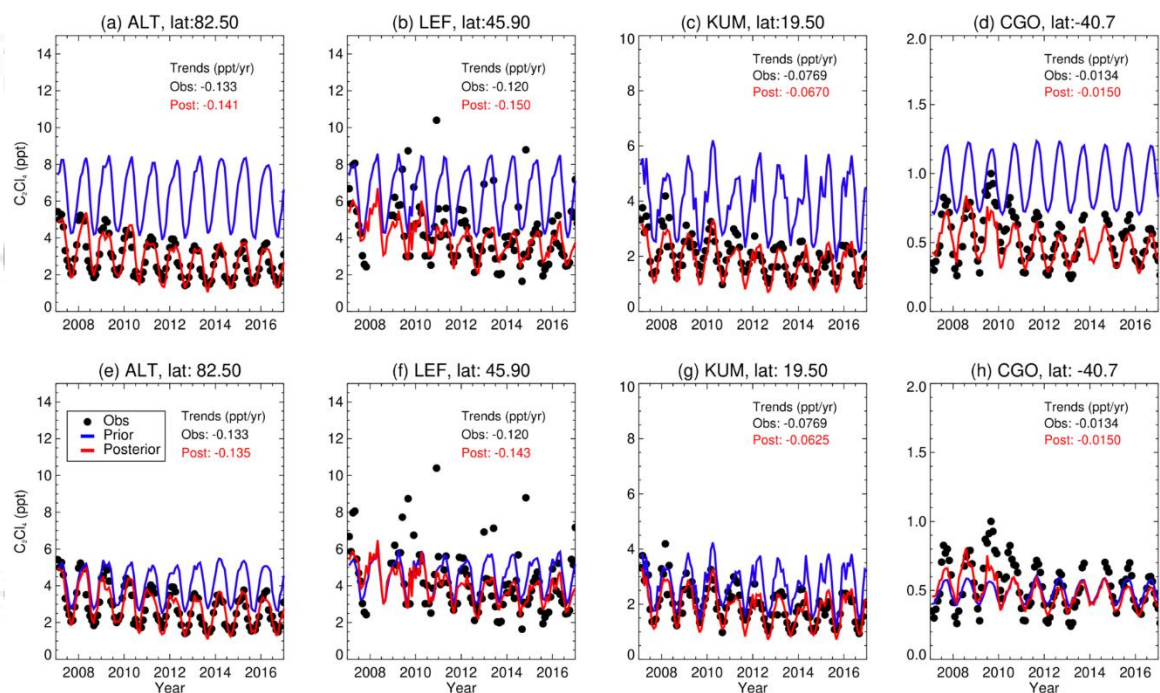


Figure 7. Comparison of modelled monthly mean C_2Cl_4 mixing ratio (ppt) versus NOAA observations (2007-2017) at the same stations as in Figure 6. Panels (a)-(d) are comparisons without the $C_2Cl_4 + Cl$ reaction, (e)-(h) are with the reaction.

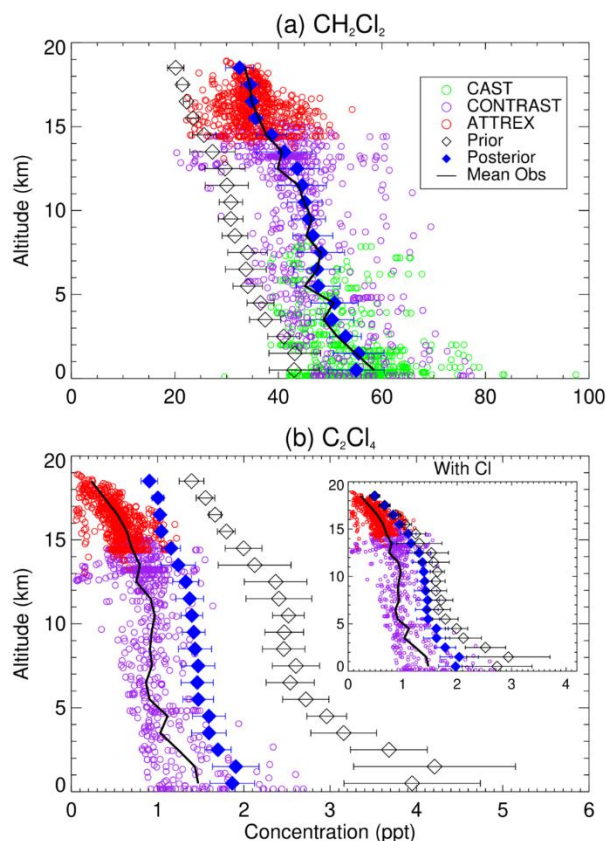


Figure 8. Modelled versus observed vertical profiles of (a) CH_2Cl_2 and (b) C_2Cl_4 volume mixing ratio (ppt) during the 2014 CAST/CONTRAST/ATTREX field missions in the West Pacific (see Section 3.2). Model output has been averaged in 1 km vertical bins and is shown for both the prior and posterior emissions. Note, these aircraft data are ‘independent’ in that they were not used in the inversion to produce the posterior emissions. The $\text{C}_2\text{Cl}_4 + \text{Cl}$ sink data are inset in (b). For CH_2Cl_2 , results are generated using the posterior emissions from the no ocean inversion scenario.

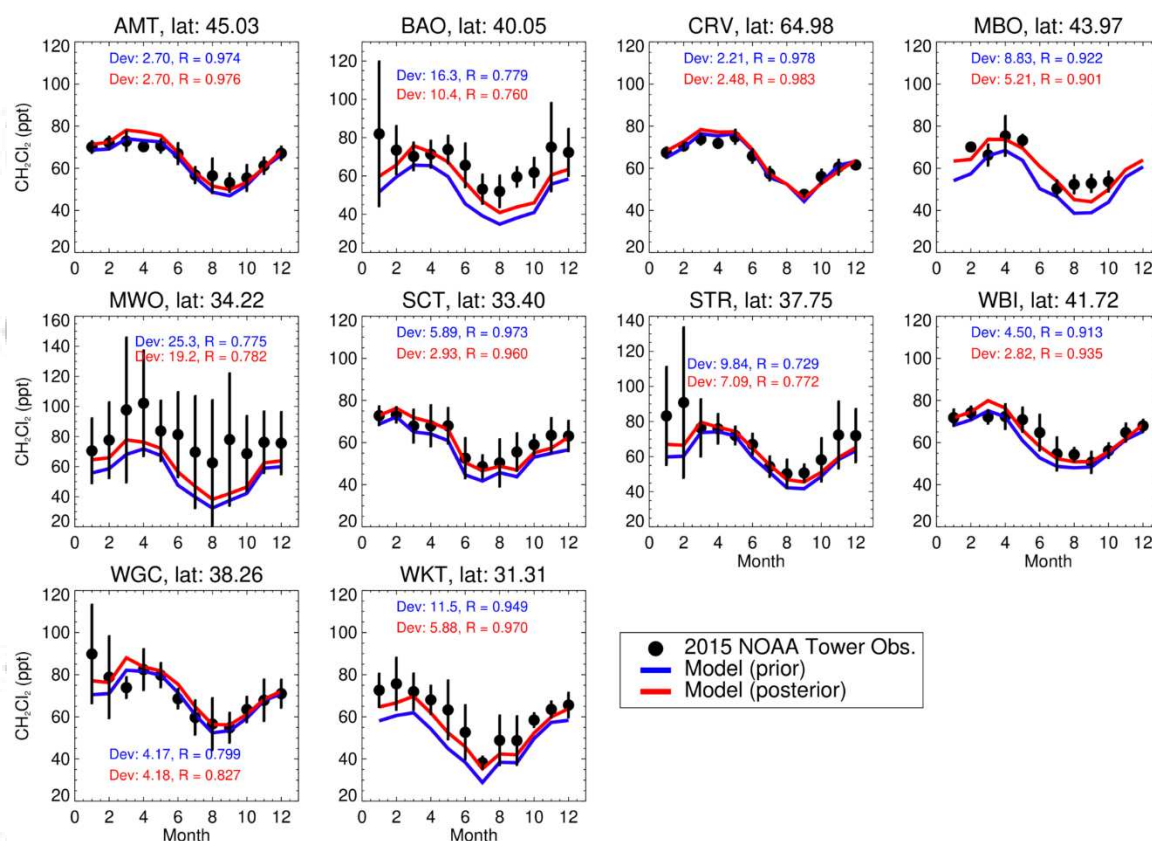


Figure 9. Comparison between monthly mean NOAA tall tower observations of CH_2Cl_2 (ppt) in 2015 (independent observations) and modelled values obtained using the prior and posterior emissions. The vertical bars on the observations indicate ± 1 s.d. of all measurements acquired at that site during that month. Annotated for each site are the average annual deviations (Dev) between the two model outputs and the observations, and the correlation coefficient, R . Results are generated using the posterior emissions from the no ocean inversion scenario.

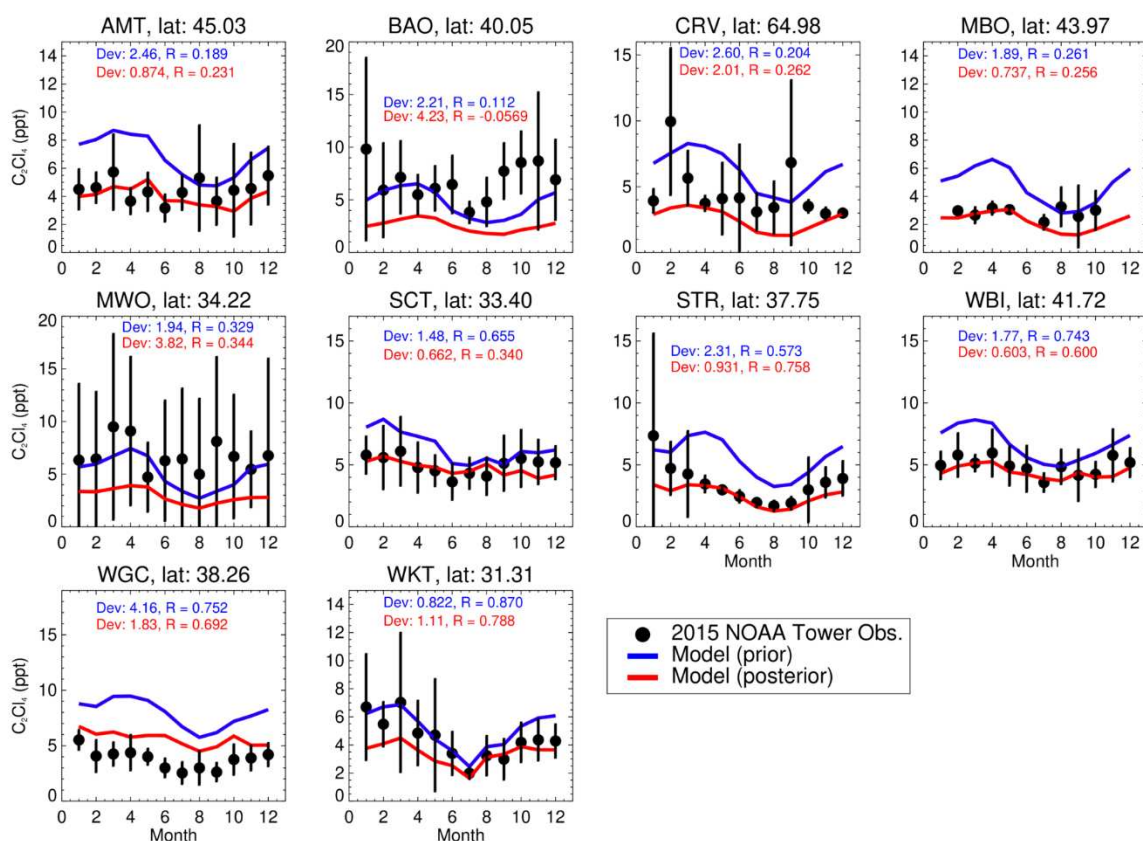


Figure 10. As Figure 9 but for C_2Cl_4 . Note, the model results here did not include the C_2Cl_4 + Cl sink.

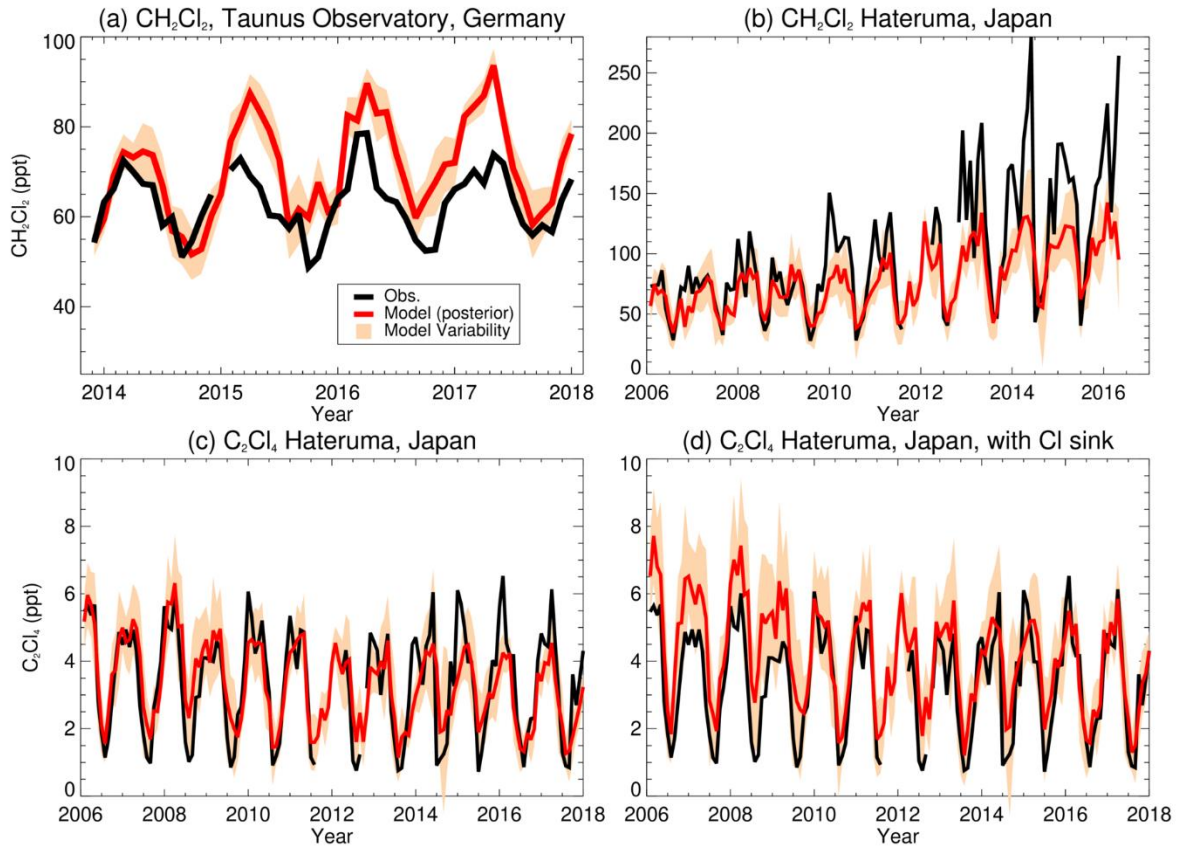


Figure 11. A comparison between modelled and observed monthly mean mixing ratios (ppt) of CH_2Cl_2 and C_2Cl_4 at independent measurement sites. (a) CH_2Cl_2 at the Taunus Observatory in central Germany [Schuck et al., 2018], (b) CH_2Cl_2 at Hateruma, Japan, (c) C_2Cl_4 at Hateruma (no $\text{C}_2\text{Cl}_4 + \text{Cl}$ sink) and (d) C_2Cl_4 at Hateruma (including $+\text{Cl}$ sink). The model output was generated using the posterior emissions from the inversion. In the case of CH_2Cl_2 , results from the no ocean inversion scenario are shown (see main text). Model variability (light orange) was calculated from the standard deviation of the surrounding 8 model grid cells (Equation 4). All observations here are calibrated to NOAA scales.